ABSTRACT

SUBBARRIER FUSION IN LIGHT AND MEDIUM HEAVY SYSTEMS

By

Jian-qun Wu

The effects of nuclear structure on subbarrier fusion in some light and medium heavy systems are studied in a two-dimensional barrier penetration model. The low-lying intrinsic excitations are represented by surface harmonic vibrations whose parameters are determined to reproduce low-lying collective excitations. The intrinsic degrees of freedom are coupled to the relative motion of two nuclei through a proximity nuclear-nuclear potential which is a function of the closest distance between two surfaces of the nuclei. We find that this model is able to explain the enhancements in subbarrier fusion observed in a variety of systems. Fusion in $^{16}O+^{18}O$ is enhanced relative to $^{16}O+^{16}O$, and this behavior is well described by the theory. In medium heavy systems, the higher overtones of the low-lying vibrations are important. We reproduce the fusion cross section in $^{46}Ti+^{90}Zr$, ^{93}Nb, $^{50}Ti+^{90}Zr$, ^{93}Nb with vibrational parameters close to those that describe transition strengths. We also studied the subbarrier fusion in the heavy systems $^{81}Br+^{90}Zr$, ^{94}Zr with only partial success. Without treating the effects due to "extra push" or "extra-extra push", the relative subbarrier

fusion of $^{81}Br+^{90}Zr$ and $^{81}Br+^{94}Zr$ are reproduced in the two-dimensional barrier penetration model. This two-dimensional model, however, fails to reproduce the absolute fusion cross section in these systems. In some systems, two-neutron transfer may play a significant role. We calculated the fusion cross section for the $^{64}Ni+^{58}Ni$ system including particle transfer channels. The form factors were obtained using a realistic microscopic model. However, the magnitude of the enhancement in this case can hardly be accounted for without a more drastic treatment of the combined effects of deformation and transfer than is conventionally assumed.

SUBBARRIER FUSION IN LIGHT AND MEDIUM HEAVY SYSTEMS

By

Jian-qun Wu

A DISSERTATION

Submitted to

Michigan State University

in partial fulfillment of the requirements

for the degree of

DOCTOR OF PHILOSOPHY

Department of Physics and Astronomy

1986

ACKNOWLEDGMENTS

First, and foremost, I wish to thank my thesis advisor, Prof. George Bertsch, for his guidance and the freedom he gave me through out the course of my graduate study at NSCL. Second, I wish to thank the remaining members of my guidance committee: Profs. Walter Benenson, Jerry Nolen, and Dan Stump. Third, I wish to thank Dr. Henning Esbensen for his constant encouragement and help over past three years. In addition, I would like to thank Drs. Don Cha, Raad Raadi, Rainer Kaps, Joe Molitoris, and Erich Ormand, who were my officemates at different times during past three years, for the helps I received. I would especially like to thank Dr. Erich Ormand for his assistance in writing this thesis. I would like to express my gratitude to Shari Conroy for her invaluable assistance and friendship through out the course of this work.

I would like to take this space to thank the Nuclear Theory Group at Oak Ridge National Laborotory and the Department of Physics & Astronomy at University of Tennesse for the hospitality and the intellectual stimulation I received during my visit from Nov., 1984 to Jun., 1985. I greatly appreciate the encouragement and advice I received from Prof. Z. R. Yu when he visited M. S. U. in 1985.

TABLE OF CONTENTS

LIST OF FIGURES..... v

LIST OF TABLES..... x

Chapter 1 Introduction..... 1

1.1 Quantum Tunneling..... 1

1.2 Subbarrier Fusion..... 4

1.3 Multidimensional Tunneling..... 6

1.4 Methods of Studying Subbarrier Fusion..... 6

Chapter 2 Models of Zero-Point Motions..... 9

2.1 Importance of Collective Excitation..... 9

2.2 Effects of Rotational Excitations..... 13

2.3 Vibrational Excitations..... 14

Chapter 3 Coupled Channel Method..... 20

3.1 Coupled Channel Treatment..... 20

3.2 Numerical Methods and Approximations..... 23

3.3 Technical Points..... 30

Chapter 4 Validity of ZPM and Simple Approximations..... 36

4.1 Validity of ZPM..... 36

4.2 Two Independent Degenerate Harmonic Oscillators..... 38

4.3 Factorization of The Enhancement Factors..... 41

Chapter 5 Subbarrier Fusion in Light Nuclei..... 44

Chapter 6 Subbarrier Fusion in Medium Heavy Nuclei..... 52

6.1 Details of The Calculation..... 52

6.2 Results and Discussions..... 56

Chapter 7 Particle Transfers in Subbarrier Fusion..... 67

7.1 Introduction..... 67

7.2 Form Factors for Neutron Transfer..... 69

7.3 Details of The Calculation..... 71

7.4 The Interplay of Intrinsic Excitations and the Particle Transfers on Subbarrier Fusion..... 76

7.5 Simultaneous Two Neutron Transfer..... 76

7.6 Discussion..... 78

Chapter 8 Conclusions..... 80

REFERENCES..... 81

LIST OF FIGURES

FIGURE

PAGE

1.1 Schematic plot of internuclear potential..... 3

2.1 A possible deformation configuration of a system of two nuclei which are spherical in their ground states..... 10

2.2 System of a spherical nucleus and a deformed nucleus separated by a distance of r..... 12

2.3 Surface vibrations of a system consisting of a "stiff" (nucleus 1) and a "soft" (nucleus 2) nuclei..... 15

2.4 Calculated and measured fusion cross sections for the reactions $^{16}O+Sm$. The abcissa is the c. m. energy $E_{c.m.}$ The samarium isotopes used are indicated, and experimental results agree with the calculations at smaller energies. There are no experimental data for ^{144}Sm. The standard deviations that have been used for the quadrupole and octupole ZPM or static deformations and the values of ΔR in eq.(2.7) are given in table 1 and 2 in ref.(Esb.81), respectively..... 17

3.1 Effects of both target and projectile zero-point motion and average dynamical deformation (Coulomb excitation) on the fusion cross section for $^{58}Ni+^{58}Ni \rightarrow ^{116}Ba$. The solid circles give the experimental data of ref.(Bec.80), the dashed curve gives the result for a one-dimensional barrier corresponding to spherical nuclei, and the solid curve gives final result for a two-dimensional potential-energy surface, and the dot-dashed curve gives the result of ZPM without dynamical

deformation..... 32

4.1 Fusion probabilities for the reaction $^{16}O+^{148}Sm$ are shown as function of the c. m. energy. The results are obtained from coupled-channel calculations, for various values of the one-phonon excitation energy $\hbar\omega$. The standard deviation of zero-point motion amplitude is $\sigma = 0.27$ fm..... 37

4.2 S-wave fusion excitation function is shown as function of c. m. energy. The dashed curve is the result obtained by combining two vibrational modes into single one through eq.(4.1). The solid line is the result obtained by solving exactly a three-dimensional coupled equation. Due to numerical restrictions, the exact result can not be obtained for energies lower than 98 MeV. The parameters are given in Table 4.1..... 40

4.3 Fusion enhancement factors are shown as functions of c. m. energy. The solid line is the result obtained by combining two vibrational modes into one through eq.(4.1). The dashed curve is the result obtained by virtue of factorization rule. The parameters used are listed in Table 4.1..... 42

5.1 The measured fusion cross section for $^{18}O+^{16}O$ and $^{16}O+^{16}O$, from ref.(Tho.85) is shown by the experimental points. The potential model fit to the $^{16}O^{16}O$ is shown as the solid line, and the coupled-channel model with rescaled potential is shown by the dashed line..... 45

5.2 Enhancement factors extracted by log-linear interpolation of the data from ref.(Tho.85). The dashed line is the

prediction of the rescaled potential, eq.(3.2). The dotted line is the prediction of the potential eq.(5.3). The solid line is the prediction of the coupled-channel model with the rescaled potential..... 46

6.1 Effective one-dimensional potential barriers for $^{13}C+^{13}C$ $^{14}N+^{14}N$, $^{13}C+^{14}O$, $^{40}Ca+^{40}Ca$, $^{64}Ni+^{64}Ni$, and $^{64}Ni+^{74}Ge$. The outer turning point is determined from the KNS potential readjusted as described in ref.(Bal.83) to fit the peak positions. The thickness is inverted from fusion cross sections and the shaded region indicates the error. The short dashed line denotes the point Coulomb potential, the long dashed curves in the upper figures denote the unmodified KNS potential, and for ease of presentation the energy is plotted relative to the barrier height..... 53

6.2 Fusion cross sections for $^{50}Ti+^{90}Zr$. The bold continuous curve is the result of the one-dimensional barrier penetration calculation. The two-channel coupling result is shown by dash-dotted curve. The thin continuous curve is the result obtained by solving 6 channel coupled equation. The 6 channels correspond to the first 6 excited vibrational states assumed in the ^{50}Ti with a energy spacing of 1.55 MeV. The dashed curve is the prediction from ZPM. All calculations include the quadrupole Coulomb excitation and ignore the angular momentum transfer..... 57

6.3 Same plot as in Fig.6.2, but for $^{46}Ti+^{90}Zr$. The parameter

V_o, Ad, ΔR are kept same as those for $^{50}Ti+^{90}Zr$. 0.89 MeV the energy of the first excited state in ^{46}Ti, is used as the energy quanta for the vibrational mode. The σ is some how 0.39 fm, different from that quoted from the B(E2) measurement..... 59

6.4 Fusion cross sections for $^{46}Ti+^{93}Nb$. The $\hbar\omega$ and σ for ^{93}Nb is taken as the average of those for ^{92}Zr and ^{94}Mo. The excitations in both ^{46}Ti and ^{93}Nb are combined into one mode with $\hbar\omega = \hbar\omega(^{46}Ti) = \hbar\omega(^{93}Nb)$ and the σ equals $\sqrt{\sigma^2(^{46}Ti)+\sigma^2(^{93}Nb)}$. The number of channels coupled is 5.. 60

6.5 Fusion cross sections for $^{50}Ti+^{93}Nb$. In the coupled channel calculation, the $\hbar\omega$ is the average of those for ^{50}Ti and ^{93}Nb. The σ is $\sqrt{\sigma^2(^{50}Ti)+\sigma^2(^{93}Nb)}$..... 61

6.6 Plot of the ratio of the fusion cross sections for $^{81}Br+^{94}Zr$ to that for $^{81}Br+^{90}Zr$. The experimental data is the cross section of evaporation residual formation..... 63

7.1 Calculated fusion cross sections for $^{58}Ni+^{64}Ni$ compared to the data of ref.(Bec.80). This plot is the copy of Fig.2(b) in ref.(Bro.83). The dotted curve shows the limit of no coupling, i.e., one-dimensional barrier penetration. The dash-dotted curve is the result obtained by including intrinsic excitations. The dashed curve includes additional channel coupling, which was attributed to transfer reaction channels..... 68

7.2 Form factor F(r) (solid line) is shown as function of the separation r. F(r-s(r)) (dot-dashed curve) is the form

factor in the semiclassical model. Also shown (dashed curve) is the largest single-particle transfer amplitude between two $f_{5/2}$ orbits in ^{64}Ni and ^{58}Ni, respectively..... 74

7.3 Fusion excitation functions of the ^{64}Ni+^{58}Ni system. Dotted curve is the result of the one-dimensional barrier penetration model. The dashed curve is the result obtained by including only intrinsic excitations with parameters given in Table 7.1. The dot-dashed curve is the result with both transfer and intrinsic excitation included. The $F_i(r-s(r))$'s are the form factors used in obtaining the result that reproduces data (solid curve)..... 75

7.4 Contours of equal density $|\psi(r,s)|^2$ are shown in the (r,s) plan. The wave function is the coupled-channel result without transfer coupling for the reaction ^{58}Ni+^{64}Ni at a c. m. energy of 90 Mev with parameters given in Table 7.1. The dotted curve is the semiclassical trajectory in which the incoming flux is maximized in the s-direction..... 77

LIST OF TABLES

TABLE PAGE

3.1 Calculated $^{50}Ti+^{90}Zr$ S-wave fusion cross sections at a c. m. energy of 100 MeV as a function of number of channels in the model space in different representations with parameters given in chapter 6..... 29

4.1 Parameters used in obtaining Fig.4.2 and Fig.4.3..... 39

6.1 Parameters of surface vibrations deduced from the measurement of low-lying states. For odd nuclei they are averages of those of two neighboring nuclei. The σ's (standard deviations) are calculated according to eq.(2.7)..... 55

6.2 Parameters of surface vibrations used in the fusion cross-section calculations of Figs.6.2,3,4,5,6. The parameters in parenthesis were obtained by fitting to the data. The rest were taken or calculated from Table 6.1.... 55

7.1 Parameters of the two-dimensional potential and the surface harmonic vibrational mode obtained by fitting the $^{58}Ni+^{58}Ni$ fusion data..... 72

Chapter 1 Introduction

1.1 Quantum Tunnelling

One of most striking features of quantum physics, the description of nature at the microscopic level, is that classically forbidden processes can occur, though generally with a small probability. Such processes are usually referred to as "tunneling" or "penetration".

Since tunneling is a classically forbidden process, it must take place with a small probability because otherwise classical physics would be of no use at all. It is indeed true that the probabilities are small. In the one-dimensional WKB approximation, the penetrability is given by (Sch.68)

$$P = 1/\{1+ \exp(-2\int_{r_1}^{r_2}\sqrt{2M/h^2(V(r)-E)}dr)\}, \qquad (1.1)$$

where $V(r)$ is the potential energy, M is the reduced mass, E is the total energy and r_1 and r_2 are classical turning points. One can see from eq.(1.1) that P is very small unless the "action" (the integral in the exponent) is small.

An analytic formula can be derived from eq.(1.1) for a parabolic potential, i.e $V(r)=V_b-\frac{1}{2}M\omega^2(r-R_b)^2$, where V_b is the barrier height and R_b is the barrier location. The penetrability is then given by (Hil.53)

$$P = \frac{1}{1+\exp[2\pi(V_b-E)/\hbar\omega]}. \qquad (1.2)$$

This procedure is also useful for the three-dimensional problem with spherical symmetry (three dimensional kinematics, but one-dimensional dynamics). Because of the relative large masses involved, it is a reasonable approximation for reactions involving heavy ions to assume that the effective centrifugal potential only changes the height of the potential barrier, and does not alter the position and the shape of the barrier. Thus, the penetrability for each partial wave can be calculated as

$$P_\ell = \frac{1}{1+\exp[2\pi(V_{b\ell}-E)/\hbar\omega]}\ , \tag{1.3}$$

where $V_{b\ell} = V_b + \frac{\ell(\ell+1)\hbar^2}{2MR_b^2}$. The total cross section (Won.73) is then

$$\sigma = \frac{\pi}{k^2}\sum_{\ell=0}^{\infty}(2\ell+1)\,P_\ell$$

$$\approx \frac{\pi}{k^2}\int_0^\infty 2\ell d\ell\, P_\ell = R_b^2\hbar\omega/2E\ \ell n\{1+\exp[2\pi(E-V_b)/\hbar\omega]\}. \tag{1.4}$$

Eq.(1.2) and therefore eq.(1.4) is valid for both $E>V_b$ and $E\leq V_b$. In the case $E>V_b$, eq.(1.4) reduces to the well-known formula:

$$\sigma = \pi R_b^2(1-V_b/E). \tag{1.5}$$

While for $E<<V_b$, we have

$$\sigma \approx R_b^2\hbar\omega/2E\ \exp[2\pi(E-V_b)/\hbar\omega]. \tag{1.6}$$

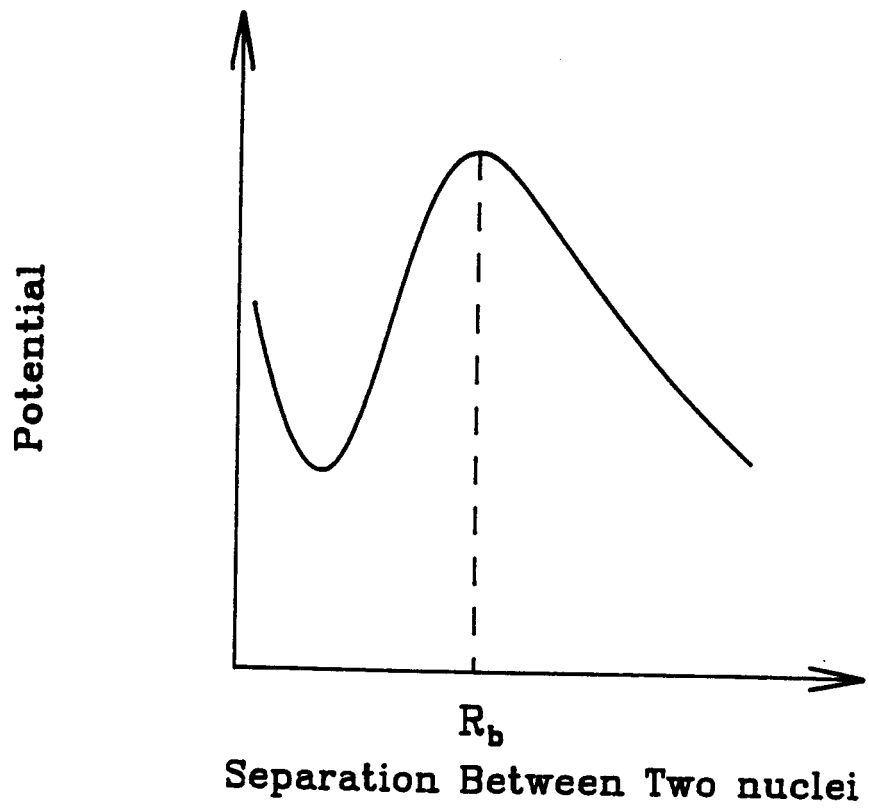

Fig.1.1. Schematic plot of internuclear potential.

Eq.(1.4)-(1.6) are very useful in computing the compound nuclear formation (fusion) cross section. As we will see, eq.(1.6), however, underestimates the fusion cross section in many cases. But it is the starting point.

1.2 Subbarrier Fusion

Potential energies between two nuclei are usually approximated as functions dependent only on the separation between the centers of mass for each nucleus. They consist of a long range Coulomb interaction and a short range nuclear interaction. A typical potential is shown in Fig.1.1. The exact potential curve depends on the system, but roughly speaking, the dip inside the barrier, called a pocket, becomes smaller as the system gets heavier. This is because the nuclear interaction is proportional to A, the number of nucleons, while the Coulomb part is $\propto Z^2 \propto A^2$. For a superheavy system (e. g. U + U), nuclear attraction is not strong enough to overcome Coulomb repulsion, and a potential pocket is not formed. For light and medium heavy systems, which are the subject of this thesis, however, the dip occurs and a barrier in between the inner and outer regions is formed. Fusion is usually assumed to happen when the system passes the Coulomb barrier. With this definition, one can use eq.(1.4) to compute the fusion cross section. For $E >> V_b$, experiments appear to agree with the law of linear inverse energy dependence given by eq.(1.5). For $E < V_b$, eq.(1.6) does not work well in general. Observed fusion excitation functions (probability or cross section as a function of bombarding energy) are much greater than those given by eq.(1.6) for energies far below coulomb barrier. This is

not because the derivation of eq.(1.6) from eq.(1.4) is wrong, but the one-dimensional approximation is insufficient. In the one-dimensional barrier penetration model (BPM), both projectile and target are assumed to be point (structureless) particles. However, nuclei may be excited during the collision. Therefore, they can not be treated as point particles.

Above-barrier fusion is a classically allowed process (in fact, it is the only final state allowed in the one-dimensional model), and intrinsic excitations of the projectile and/or the target does not change the order of magnitude of the above-barrier fusion cross section. Thus, eq.(1.5) can be used. Intrinsic excitations, however, may alter other observations, such as elastic and inelastic angular distributions. As far as above-barrier fusion is concerned, the one-dimensional model is a good approximation.

How intrinsic excitations effect subbarrier fusion is an entirely different story. It will be seen in chapter 2 that intrinsic excitations can change the order of magnitude and the shape of subbarrier fusion excitation function. There are some systems for which eq.(1.5) works for energies just below the Coulomb barrier. In general, however, heavy-ion subbarrier fusion is a multidimensional tunnelling process (Lec.84).

One motivation for studying heavy-ion subbarrier fusion is to search for superheavy elements. These superheavy elements decay very rapidly into smaller components, even in their ground state. So they have to be made with energies as low as possible in order to make them live longer to make experimental study feasible. This leads to the study of subbarrier fusion. At the moment, the heaviest elements are

all very shortly lived, and can not be made as targets in experiments in seeking heavier elements. Thus, heavy-ions (usually referred to any ion heavier than α-particle) as both targets and bombarding particles are required.

1.3 Multidimensional Tunneling

An appreciation of the underlying physics is crucial in deriving the results of WKB approximation (eq.(1.1)). From a practitioner's point of view, however, the approximation is not that crucial in the sense that with modern computers one can perform a straightforward one-dimensional integral to obtain the penetrability. The numerical calculation of multidimensional tunnelling, on the other hand, is very difficult. Therefore, although one can not obtain an analytical formula, as in the WKB in one-dimensional case, approximations based on the underlying physics are absolutely necessary.

On the theoretical side, in addition to reproducing experimental data, the study of multidimensional tunnelling is a interesting subject in itself and subbarrier fusion provides a test on our understanding of the subject.

1.4 Methods of Studying Subbarrier Fusion

For light and medium heavy systems, measurements of subbarrier fusion can be made directly by measuring the evaporation residue because particle emmision dominates fission in the compound decay. In such experiments, one measures the charge or the mass or both of the reaction

products, directly or indirectly (e. g. Gut.73, Püh.75, Nat.70, Bro.75, Sto.81). For heavy systems, fission is the dominant channel for compound system decay. In this case, there is no evaporation residue, so the fusion yield is measured by measuring fragment coincidences. In such experiments, one must know beforehand the properties of the fragmentation of the compound systems. In general, fusion experiments of heavy systems consist of more sophisticated measurements than direct measurements in lighter systems.

Theoretically, as mentioned in the previous section, exact calculations are very difficult. Almost all subbarrier fusion excitation functions fall off exponentially as bombarding energy decreases except in very few systems where resonances exist. The key parameter is the energy in the center of mass (c.m.) frame. This enables one to make very useful approximations. As an example, we will see in Chapter 3, that one can make approximations about angular momentum algebra based on energy considerations.

The principle reason why eq.(1.6) fails is that nuclei may be excited during the collision. Therefore one has to go beyond the one-dimensional barrier penetration model (BPM). The two-dimensional zero-point motion models (ZPM) which take into account the barrier fluctuations due to intrinsic excitations have been very successful in describing subbarrier fusion for some systems. In next chapter, ZPM will be described. Following that in chapter 3, we will discuss the more general two-dimensional model, namely, coupled-channel formulations and approximations used to solve the coupled equations. In chapter 4, the validity of ZPM will be tested, and approximations for reducing three- or more-dimensional problems to two-dimensional ones will be

studied. Chapter 5 and chapter 6 contain the results of calculations and discussions of subbarrier fusion in some light and medium heavy systems. Effects due to particle transfer on subbarrier fusion will be studied for system of Ni+Ni in chapter 7. Finally, we conclude in chapter 8.

Chapter 2 Models of Zero-Point Motions

The simplest two-dimensional models are zero-point motion models. In these models, the intrinsic excitation energy is assumed to be zero. The idea is that only low-lying collective excitations are important, so the excitation energies are small, and can be neglected completely. There are two kinds of models associated with two different modes of collective excitations, namely vibrations and rotations. In sec.2.1, we will first discuss why collective excitations play an important role in subbarrier fusion. Sec.2.2 contains a description of the rotational averaging model which takes into account the rotational excitation in a well-deformed nucleus. In sec.2.3, the vibrational zero-point motion model will be discussed.

2.1 Importance of Collective Excitation.

There are two reasons why collective excitations are an important degree of freedom in subbarrier fusion. One is that low-lying collective states have smaller excitation energies than other kinds of excitations, say single-particle excitations. If the excitation energy is large, then the energy of the relative motion of the two nuclei is much smaller than that in the entrance channel. Therefore, the excitation gives little contribution to the process of subbarrier fusion. One can see this more clearly in following way: if the internal excitation happens during the collision of two nuclei, the potential is no longer a local one-dimensional one, rather a multidimensional matrix. When it is diagonalized, a number of eigenvalues will be smaller than

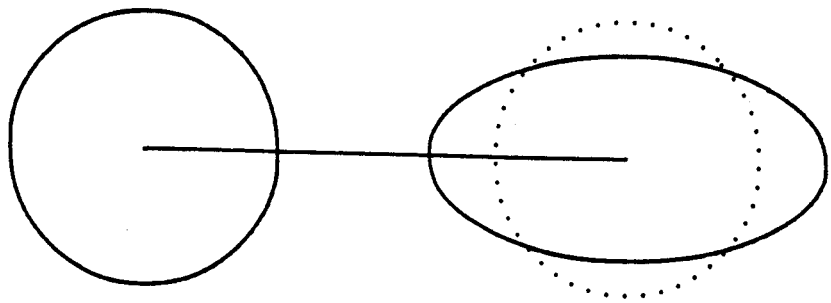

Fig.2.1. A possible deformation configuration of a system of two nuclei which are spherical in their ground states.

the potential in the entrance channel. It is this effect which can enhance subbarrier fusion reactions. On the other hand, if the internal excitation energy is large (the difference between two neighbor diagonal elements in the potential matrix is large), the lowest eigenvalue of the potential matrix would be essentially same as that in the entrance channel. Thus, it is not possible for excitations to contribute significantly.

The second reason is that collective excitations are more strongly coupled to the relative motion than other intrinsic excitations. Many particles move coherently in a collective excitation, which changes the internuclear potential substantially. If the off-diagonal elements (couplings) in the potential matrix are large, the lowest eigenvalue of the potential matrix is much lower than the potential in the entrance channel, and subbarrier fusion can be enhanced substantially.

There is a physical picture which explains why low-lying collective excitations are important in subbarrier fusion.

Suppose two nuclei are deformed as shown in Fig.2.1. Though the deformation take some energy away from the relative motion, if r is within the range of nuclear force, the attractive nuclear potential is much stronger than if there is no deformation. This "extra" attraction makes the barrier lower than if the two nuclei were in their ground states, and leads to enhancement in subbarrier fusion. In order to make this mechanism work, the excitation energy must be small and the "extra" nuclear attraction must over-compensate the loss of the energy for the relative motion. Only low-lying collective excitation can fulfill these two requirements. Note, however, that the Coulomb force works against this.

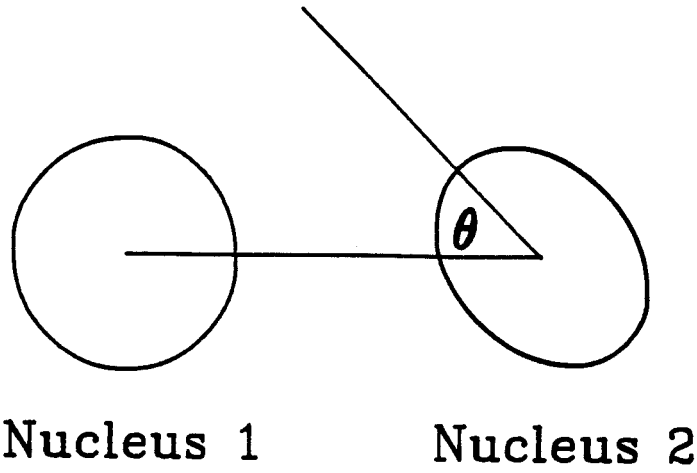

Fig.2.2 System of a spherical nucleus and a deformed nucleus separated by a distance of r.

2.2 Effects of Rotational Excitations.

Now we consider a subbarrier fusion reaction between two heavy ions. Here we take one nucleus to have a well-deformed ground state, while the other possesses spherical symmetry. The lowest possible internal excitation for this system is a rotational excitation of the deformed nucleus. In this case, the potential is no longer one-dimensional, but at least a function of two dimensions. As shown in Fig.2.2, the potential is a function of the relative coordinate r and the angle θ between the symmetric axis of the deformed nucleus and the relative coordinate.

Wong (Won.73) has calculated the fusion cross-section for such systems. Instead of following the details of his work, we give a rough estimate to show what effect averaging over the angle θ has on subbarrier fusion.

The Coulomb barrier height V_b can be written as

$$V_b = \bar{V}_b + f(\theta),$$

where $\bar{V}_b$ is the averaged barrier height and $f(\theta)$ is some function with

$$\int f(\theta)\, d\theta = 0.$$

The subbarrier fusion cross section σ_{fus} , in the WKB approximation, is an exponential function of V_b and E_{cm} (the energy of the relative motion in the c. m. frame), namely

$$\sigma_{fus}(\bar{V}_b,\theta) \propto e^{-(V_b(\theta)-E_{cm})c}, \tag{2.1}$$

where c is some positive number. The averaged cross section is then

$$\bar{\sigma}_{fus} = \int d\theta\ \sigma_{fus}(\bar{V}_b,\theta) \propto e^{-(\bar{V}_b-E_{cm})\,c}\ \frac{\int d\theta\ e^{-f(\theta)\,c}}{\int d\theta}, \tag{2.2}$$

where the uniform distribution over θ is assumed and the reaction is incoherent in θ, that is, θ does not change during a collision, which, we will see later, corresponds to the zero excitation energy limit. If $\frac{\int d\theta\ e^{-f(\theta)c}}{\int d\theta}$ is greater than one (it turns out that it is the case if $E_{cm} < \bar{V}_b$), then $\bar{\sigma}_{fus} > \sigma_{fus}(\bar{V}_b)$, that is, the subbarrier fusion cross section is enhanced.

In general the rotational excitation energy is not zero, but small, and therefore can be approximated as zero for some heavy systems.

2.3 Vibrational Excitations.

For spherical nuclei, the lowest excitations are surface vibrations. Thus subbarrier fusion of two spherical nuclei is enhanced mainly due to vibrational excitations in the nuclei. In general, the vibrational excitations are not purely harmonic, however, we will assume that this is the case for the purpose of simplicity.

The picture here is the same as that in sec.2.2 : The potential is a two variable function. The first variable is the distance between the centers of the two nuclei r, while the second is the vibrational surface-collective variable s.

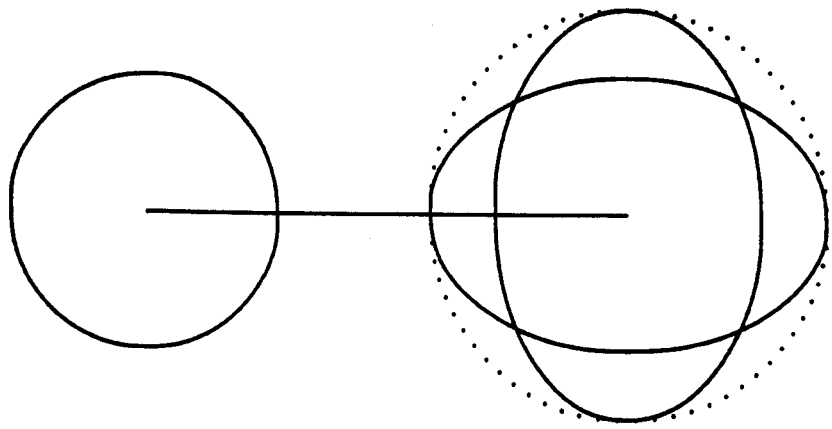

Fig.2.3. Surface vibrations of a system consisting of a "stiff" (nucleus 1) and a "soft" (nucleus 2) Nuclei.

The nucleus deforms around the equilibrium spherical shape. Because of the isotopy of the space, on the average the nuclear surface vibrates as shown by dashed circle in Fig.2.3. For a positive s there is more nuclear attraction than if s=0, and there is even less nuclear attraction for negative s. If the intrinsic excitation energy is small, and can be approximated as zero, the fusion cross section is that averaged over s with some weight determined by the asymptotic boundary condition. Again due to the exponential fall-off of subbarrier fusion cross section (eq.(2.1), the subbarrier fusion is usually enhanced.

Esbensen (Esb.81) used this model to calculate subbarrier fusion cross sections of ^{16}O+Sm and Ar+Sm. This model was very successful in explaining the experimental data, which were much larger than the results given by conventional penetration model. In these systems, the targets (Sm isotopes) have low-lying vibrational excitations, and the intrinsic excitations were assumed to be only in the targets.

The Schrödinger equation in ZPM can be written as

$$\left[\frac{P^2}{2m} + V(r,s)\right] \psi(r,s) = E_{cm}\, \psi(r,s). \qquad (2.3)$$

Since there is no differential operator in s, this equation can be solved by treating s as a parameter and solving the one-dimensional equation for r. There is no correlation in s, so nuclei bombarding with a different s scatter incoherently, i. e., s does not change during the collision. This is sometimes called the frozen approximation. In this approximation the penetrability is

$$P(E_{cm}) = \int ds\, P(E_{cm}, s)\, B(s), \qquad (2.4)$$

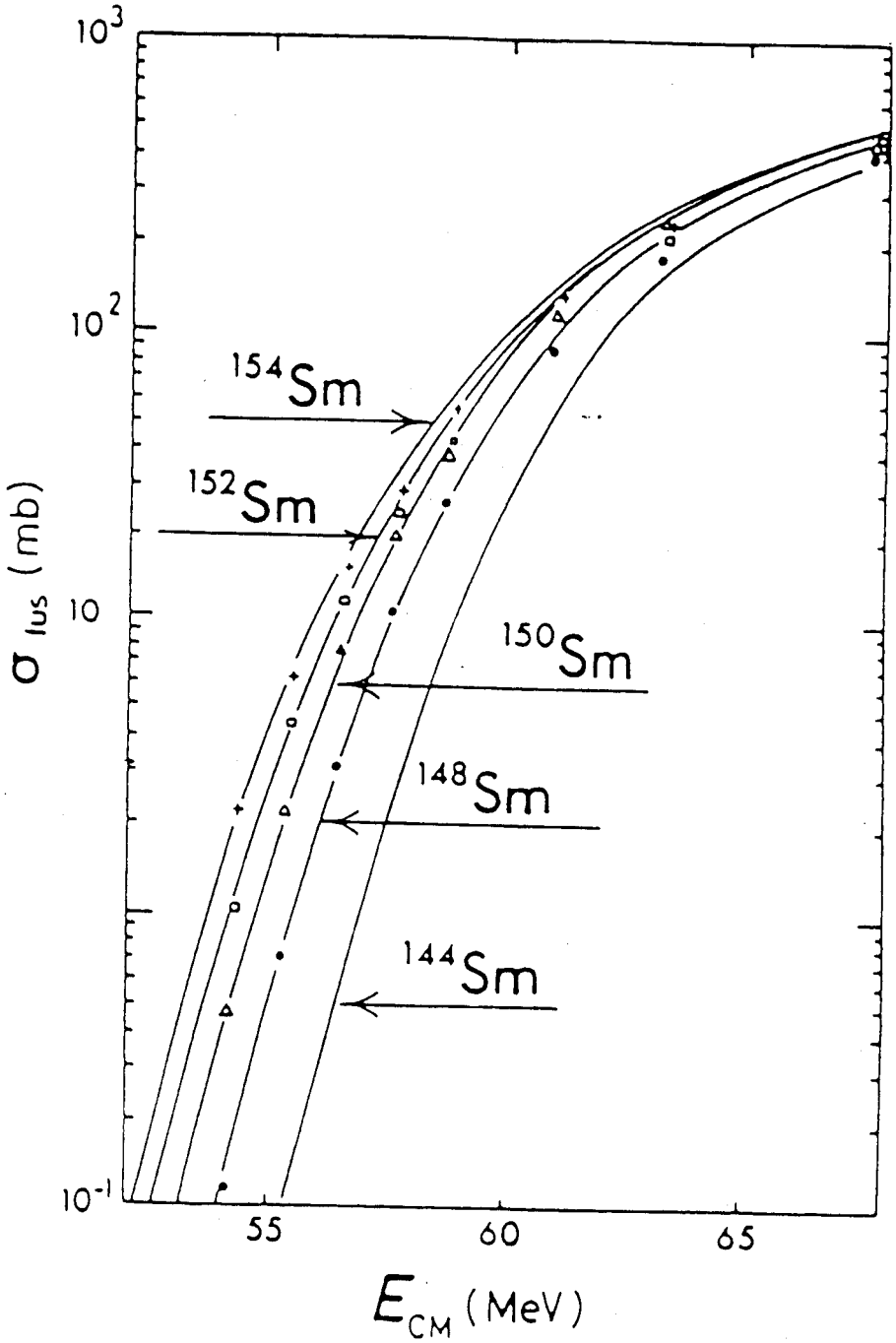

Fig.2.4. Calculated and measured fusion cross sections for the reactions ^{16}O+Sm. The abcissa is the c.m. energy $E_{c.m.}$. The samarium isotopes used are indicated, and experimental results agree with the calculations at smaller energies. There are no experimental results for ^{144}Sm. The standard deviations that have been used for the quadrupole and octupole ZPM or static deformations and the values of ΔR in eq. (2.6) are given in table 1 and in table 2 in ref. (Esb.81), respectively.

where $P(E_{cm},s)$ is the penetration factor for the potential $V(r,s)$, which can be calculated by eq.(1.4), $B(s)$ is determined by the asymtotic boundary condition. Usually the target is in its ground state, therefore $B(s)$ is a gaussian, i. e.

$$B(s) = \frac{1}{\sqrt{2\pi}\sigma} e^{\frac{s^2}{2\sigma^2}}, \tag{2.5}$$

where σ is the r. m. s. amplitude of the surface vibrational ground state of the target. For subbarrier fusion, $P(E_{cm})$ is usually much greater than that if there is no coupling of the surface motion to the relative motion.

In Fig.2.4, the calculated fusion cross sections of ^{16}O+Sm in this model are compared with the data (Sto.80). The nuclear potential used was

$$U(r,s) = V_0 \frac{R_1R_2}{R_1+R_2} \frac{1}{1+\exp[(r-R_1-R_2-\Delta R-s)/a]}. \tag{2.6}$$

The parameters V_0 and a were extracted from elastic scattering data (Chr.76), and ΔR was adjusted to fit the fusion data. In the calculation, the monopole, quadrupole, and octopole Coulomb interaction were included in the potential. The σ's were extracted from the low-lying state data through (Esb.81)

$$\sigma_\lambda = \frac{R}{Z(\lambda+3)} \left((2\lambda+1) \frac{B(E\lambda)}{B_W(E\lambda)}\right)^{1/2} \tag{2.7}$$

where λ denotes the multipolarity, $B(E\lambda)/B_w(E\lambda)$ is the electric transition strength in terms of Weisskopf unit and R and Z are the radius and charge number of the Sm-isotope, respectively. In this case, angular momentum transfer was ignored. As can be seen in the figure, the agreement is very good in the subbarrier region.

Chapter 3 Coupled Channel Method

There is one thing in common in Wong (Won.73) and Esbensen (Esb.83)'s work: the intrinsic excitation energy is assumed to be zero. This is a good approximation for some heavy systems, but questionable in general. In these models, the two dimensional equation is essentially one-dimensional, so it is easy to do numerical calculations. Intuitively, the ZPM can only be an approximation. The more general formulation of the two-dimensional model with finite intrinsic excitation energy, namely the coupled channel formulation will be given in sec.3.1. In sec.3.2 various numerical methods and approximations for solving coupled-channel equations are presented. The Coulomb excitation and angular momentum transfer will be discussed in sec.3.3.

3.1 Coupled Channel Treatment

We know from the previous chapter that collective excitations enhance the subbarrier fusion. The simplest realistic Hamiltonian is at least two-dimensional. In this section, we present the coupled-channel formulation for a system in which the surface vibrational degree of freedom is important.

The two-dimensional Hamiltonian can be written as

$$H(r,s) = \left(- \frac{\hbar^2}{2m} \nabla^2 + H_{in}(s) + V(r,s) \right), \qquad (3.1)$$

where m is the reduced mass, $H_{in}(s)$ is the surface vibrational Hamiltonian in nucleus 1. $V(r,s)$ is composed of Coulomb and nuclear interactions, i. e.

$$V(r,s) = \frac{Z_1 Z_2 e^2}{r} + \frac{3Z_1 Z_2 e^2 R_1 s}{5r^3} + V_0 \frac{R_1 R_2}{R_1 + R_2} \operatorname{erf}\left(\frac{r-R_1-R_2-\Delta R-s}{a}\right), \quad (3.2)$$

where the second term is the quadrupole Coulomb excitation. The complementary error functional form was used for convenience in numerical computation. The parameters V_0, a, R_i and ΔR are taken as

$$V_0 = -31.61 \text{ MeV}, \quad a = 1.42 \text{ fm},$$
$$\Delta R = 0.29 \text{ fm, and } R_i = 1.233\, A^{\frac{1}{3}} - 0.98\, A^{-\frac{1}{3}}, \quad (3.3)$$

and were extracted from elastic scattering data (Chr.76).

To solve the two-dimensional Schrödinger equation

$$H(r,s)\, \psi(r,s) = (E + \tfrac{1}{2}\hbar\omega)\, \psi(r,s), \quad (3.4)$$

where E is the total energy of both the relative motion in the c. m. frame and the intrinsic excitation, we expand the wave function on a set of oscillator eigenfunctions $\phi_n(s)$ of $H_{in}(s)$

$$\psi(r,s) = \sum_n \psi_n(r)\, \phi_n(s) \quad (3.5)$$

and obtain the coupled equations

$$\left\{-\frac{\hbar^2}{2M}\frac{\partial^2}{\partial r^2} + \langle n|V|n\rangle - E + n\hbar\omega\right\} \psi_n(r) = -\sum_{m \neq n} \langle m|V|n\rangle\, \psi_m(r). \quad (3.6)$$

The matrix elements $\langle n|V|m\rangle$ are given by

$$\langle n|V|m\rangle = \int ds\ \phi_n(s)\ V(r,s)\ \phi_m(s). \tag{3.7}$$

The boundary conditions are incoming waves at a certain c. m. distance r_{min} near the minimum of the total interaction or decaying states, when $E-n\hbar\omega$ is less than the total interaction energy at r_{min} and Coulomb wave functions at $r=r_{max}$ outside the barrier, where the nuclear fields vanishes, i. e.

$$\psi_n(r) \longrightarrow \begin{cases} P_n\, e^{-ik_n(min)\, r} & r \leq r_{mi} \\ \delta_{n0}\psi_{c\,n}^{(-)}(r) + R_n\psi_{c\,n}^{(+)}(r) & r \geq r_{ma} \end{cases} \tag{3.8}$$

Here $\hbar k_n(min)$ is the radial momentum at r_{min} in the n^{th} channel and $\psi_{c\,n}^{(\pm)}(r)$ represents outgoing and incoming Coulomb wave function in different channels with an energy of $E-n\hbar\omega$ in the relative motion. There is only an incoming Coulomb wave function in the elastic channel. The fusion probability P_{fus} is the sum over all channels of the relative flux at r_{min} in each channel, that is

$$P_{fus} = \sum_n |P_n|^2\, \hbar k_n(min)/\sqrt{2Em}. \tag{3.9}$$

In principle, the coupled-channel formulation is equivalent to eq.(3.1) if a complete set of oscillator eigenfunctions $\phi_n(s)$ is used in the expansion. In practice, however, a finite set is used in order that the calculation is feasible.

In next section, we will discuss several methods and approximations for solving the coupled equations in eq.(3.6).

3.2 Numerical Methods and Approximations

We first start with the method of iteration. This method has been used by Rhoades-Brown et al. (Rho.84) in subbarrier fusion calculations. It works like this: first, the solution satisfying the outer boundary condition (at $r=r_{ma}$) in eq.(3.8) is guessed. The solution is used for the right-hand side (RHS) of eq.(3.6). By calculating the LHS of eq.(3.6), a new solution is obtained. Then, the new solution is used for the RHS to obtain a newer solution. One repeats this process until a pre-set convergence test is achieved. In the calculation, an additional short range imaginary potential is added to the Hamiltonian (eq.(3.1)) to replace the inner boundary condition. Unfortunately, the method of iteration does not guarantee a converged solution. Various tricks have been invented to improve this procedure. The method described above is the simplest, called sequential iteration, in which the RHS is kept fixed while solutions in all channels are obtained. An improved method is called block iteration, in which a solution in a channel is immediately substituted into the RHS with some modifications when they are necessary to satisfy the boundary condition. In addition, Pade approximments have also been used by Rhoades-Brown et al. (Rho.80). This method works for some problems which can not be solved by either the simple sequential or block iteration techniques. But, again, there is no guarantee. For subbarrier fusions, calculations are often time

consuming, and a converged solution can not be obtained when the fusion cross section is down below the o.1 mb level (Rho.84).

The direct matrix inversion method has been used by Ring et al. (Rin.78) in calculating subbarrier fission penetrability. It has also been used by Esbensen et al. (Esb.83) in subbarrier fusion calculation. Instead of using an additional imaginary potential, an incoming wave boundary condition is imposed at a distance inside the Coulomb barrier. This represents the same physics as that represented by the short range imaginary potential used in iteration method: Once the system passes the Coulomb barrier, fusion take place with a 100% probability. By solving eq.(3.6), one obtains a matrix connecting the inner boundary condition and outer boundary condition. By inverting the matrix, the fusion probability is obtained. Mathematically, it works as follows. Suppose the total number of channels is N. So there are N independent solutions to eq.(3.6) satisfying the inner boundary conditions given in eq.(3.8). But only one solution satisfies both inner and outer boundary conditions given in eq.(3.8) which can be obtained in the following way:

One solves eq.(3.6) with

$$\psi_{i,n}(r) = \delta_{in} \exp(-ik_n(min)\, r) \quad \text{at } r=r_{mi} \qquad i=1,2,\cdots N, \qquad (3.10)$$

where i denotes the channel number and n denotes the specific boundary condition. At $r=r_{ma}$, one obtains

$$\psi_{j,n}(r) = B_{j,n}\psi_{c\,j}^{(-)}(r) + D_{j,n}\psi_{c\,j}^{(+)}(r) \qquad j=1,\ 2,\cdots N \qquad (3.11)$$

where n denotes the specific boundary condition in eq.(3.10) and j denotes the channel number. n assumes values 1,2,....N, giving N independent solutions. The general solution satisfying the inner boundary condition given in eq.(3.8) is a linear combination of these solutions

$$\psi_j(r) = \sum_{n=1}^{N} P_n \psi_{j,n}(r), \tag{3.12}$$

where the P_n's are coefficients. To achieve a solution that satisfies the outer boundary condition, one finds coefficients P_n, such that

$$\begin{bmatrix} B_{1,1} & B_{1,2} \cdots\cdots\cdots & B_{1,N} \\ B_{2,1} & B_{2,2} \cdots\cdots\cdots & B_{2,N} \\ \cdots\cdots\cdots\cdots\cdots & & \\ \cdots\cdots\cdots\cdots\cdots & & \\ B_{N,1} & B_{N,2} \cdots\cdots\cdots & B_{N,N} \end{bmatrix} \begin{bmatrix} P_1 \\ P_2 \\ \cdot \\ \cdot \\ P_N \end{bmatrix} = \begin{bmatrix} 1 \\ 0 \\ 0 \\ \cdot \\ 0 \end{bmatrix}, \tag{3.13}$$

and, therefore, we have

$$\begin{bmatrix} P_1 \\ P_2 \\ \cdot \\ \cdot \\ P_N \end{bmatrix} = B^{-1} \begin{bmatrix} 1 \\ 0 \\ 0 \\ \cdot \\ 0 \end{bmatrix}. \tag{3.14}$$

The fusion probability is then determined with eq.(3.9).

With this procedure there is no convergence problem. However, numerical precision can quickly become a limiting factor when the number of channels increases.

Below the barrier the matrix to be inverted has elements which differ by several orders of magnitude. This is because wave functions in various channels are exponential functions with different decay lengths. Therefore, elements of B differ by orders of magnitude for energy far below the barrier. The transmission factor (penetrability) can be written as

$$P = p + \varepsilon \tag{3.15}$$

where little p is the true value of the transmission factor and ε is the numerical error that comes out of a numerical calculation. A simple estimate of the error can be made for a simplified model:

Suppose the potential barrier is a square potential characterized by its height V_b and its width a. The error in the transmission factor obtained by the direct matrix-inversion method described above is of the order of

$$\varepsilon \approx \frac{\exp((\alpha'-\alpha)a)}{10^m}, \tag{3.16}$$

where α' and α are wave numbers under the barrier in channels with the least and the largest energies for relative motion, respectively. And m is the number of effective digits that can be handled by the computer used. Substituting eq.(3.16) into eq.(3.15), one obtains

$$T = t\left(1+\frac{\exp((\alpha'-\alpha)a)}{t\ 10^m}\right). \qquad (3.17)$$

As the energy goes down, the relative error becomes larger. At some point, one can not use the direct matrix inversion method any more.

The precision limitation may be overcome by a step-wise inversion method. That is, one divides the barrier into several intervals and constructs transmission matrices for each segment. The total transmission factor is

$$P = \prod_{i=1}^{n}\left(p_i+\frac{\exp((\alpha'-\alpha)a/n)}{10^m}\right) = \prod_{i=1}^{n} p_i\left(1+\frac{\exp((\alpha'-\alpha)a/n)}{p_i\ 10^m}\right)$$

$$\approx P\left(1 + n\,P^{(n-1)/n}\exp(-(\alpha'-\alpha)\frac{n-1}{n}a)\quad\frac{\exp((\alpha'-\alpha)a)}{P\ 10^m}\right), \qquad (3.18)$$

where n is the number of segments and little p_i is the transmission factor for i^{th} segment. In obtaining eq.(3.18), the barrier has been sliced into equal parts and the transmission factor has been assumed to be the same for each segment and P ($= p_i^n$) is the true total transmission factor. The factor $n\,P^{(n-1)/n}\exp(-(\alpha'-\alpha)\frac{n-1}{n}a)$ is less than one and decreases as n increases. Compare eq.(3.17) with eq.(3.18), one finds that the error can be reduced by the step-wise matrix inversion method.

The adiabatic representation is also very efficient, and has been used in subbarrier fusion calculations (Tan.85). To illustrate, let us first rewrite eq.(3.6) in a more compact form:

$$\left(\frac{h^2}{2M}\frac{\partial^2}{\partial r^2} + V(r)-E\right)\psi(r)=0, \qquad (3.19)$$

where $\psi(r)$ is an N-dimensional vector (N is the total number of channels explicitly treated in the calculation). Each component $\psi_i(r)$ is the wave function in channel i and V(r) is a N×N potential matrix with off-diagonal elements given by eq.(3.7). The diagonal elements are given by eq.(3.7) plus the intrinsic excitation energies. The coupled channel basis is transformed to diagonalize V(r) at each point. Then eq.(3.19) becomes

$$\left(-\frac{\hbar^2}{2M} D(r) \frac{\partial^2}{\partial r^2} D^{-1}(r) + D(r)V(r)D^{-1}(r) - E\right) D(r)\Psi(r) = 0, \qquad (3.20)$$

where D(r) is the transformation matrix and $D(r)V(r)D(r)^{-1}$ is diagonal. In this representation, only the first few channels are needed to accurately calculate the subbarrier fusion cross section. Therefore, the basis is usually truncated to a few states with the lowest energies. If the space is truncated to a single state and the derivatives of D^{-1} are dropped in the kinetic energy operator, we obtain the well-known adiabatic approximation. This limit is employed in the subbarrier fusion calculations of Tanimura et al. (Tan.85). The advantage of using the adiabatic representation can be seen in a numerical example demonstrated in Table 3.1, comparing the S-wave fusion cross sections for $^{50}Ti + ^{90}Zr$ under various truncations. The first 5 states in the entrance channel representation define the space. One would expect the results to be independent of the representation if the full space is used. From the last row of the Table, we see that this is not quite the case; the definition of an incoming-wave boundary condition depends somewhat on the representation. The adiabatic representation shows that a 2-state truncation has converged, although a 1-state truncation is

Table 3.1. Calculated $^{50}Ti+^{90}Zr$ S-wave fusion cross sections at a c. m. energy of 100 MeV as a function of number of channels in the model space in different representations with parameters given in chapter 6

No. of channels	Representation		Adiabatic
	Entrance	Adiabatic	Approximation
1	0.03 μb	18.4 μb	46.7 μb
2	0.98 μb	6.65 μb	
3	3.45 μb	6.45 μb	
5	5.61 μb	6.51 μb	

quite poor. The adiabatic approximation, which is a 1 state truncation with the entrance channel kinetic operator, works poorly in this case. In the entrance channel representation, several states are needed. If a factor of two is tolerable in the accuracy, the space can be truncated to three channels. This is consistent with the findings of Takigawa, et al. (Tak.85)

Sec.3.3 Technical Points

In this section, we discuss the effects of the Coulomb excitation and angular momentum transfer between intrinsic degree of freedom and the relative motion. The reason we discuss these effects is that the amount of computation can be reduced a great deal if one can make some approximations about these. We start first by studying Coulomb excitation.

Let us begin with a qualitative discussion. First, the Coulomb field reduces the enhancement due to nuclear multipole forces. The reason is that the nuclear force is attractive, while the coulomb interaction between positive charges (protons) is repulsive. In a subbarrier reaction, the nuclear force tends to change the shapes of the nuclei to have a stronger attraction. The Coulomb force, on the other hand, changes the shapes to reduce the repulsion. In other words, two fields prefer different shapes. Due to the saturation of nuclear interaction, the Coulomb force becomes more important as system becomes heavier. Roughly speaking, the strength of the nuclear interaction is proportional to A, the number of nucleons involved. While the Coulomb

strength goes as $\propto A^2$. As a matter of fact, the effects of the extra-push to be discussed in chapter 6 is mainly due to relative importance of the Coulomb force in heavy systems.

Multipole components of the Coulomb force introduce some complications in numerical calculations. Unless one uses the adiabatic approximation (Rho.80), one has to integrate the coupled equations to a large separation because of the long-range of the Coulomb interaction. And if there were no Coulomb multipole force, the subbarrier fusion would be easily estimated in a multichannel WKB approximation.

Landowne (Lan.81) showed numerically that Coulomb multipole interactions work against nuclear attractions in subbarrier fusion reactions. In his model, in classically allowed region he assumed a classical trajectory in the two-dimensional space (r,s) for the system. The zero-point fluctuations of s were assumed to be the same as without multipole Coulomb forces, but the center of s was determined by the trajectory. Under the barrier, the frozen approximation was used to calculate the penetrability. Essentially the fusion cross section is given by eq.(2.4) with s in the integrand replaced by $s-s_0$, s_0 being the value of the variable of the intrinsic degree of freedom at the classical turning point. s_0 is nonzero due to the Coulomb excitation.

In Fig.3.1, the results in different models are compared. The ZPM without tne inclusion of the Coulomb excitation (dash-dotted curve) enhances the subbarrier fusion substantially. The ZPM with the Coulomb excitation included (solid line) reduces the enhancement. The net enhancement is almost negligible. Therefore in heavy systems, Coulomb excitation is very important. However, in lighter systems, e.g. O+O

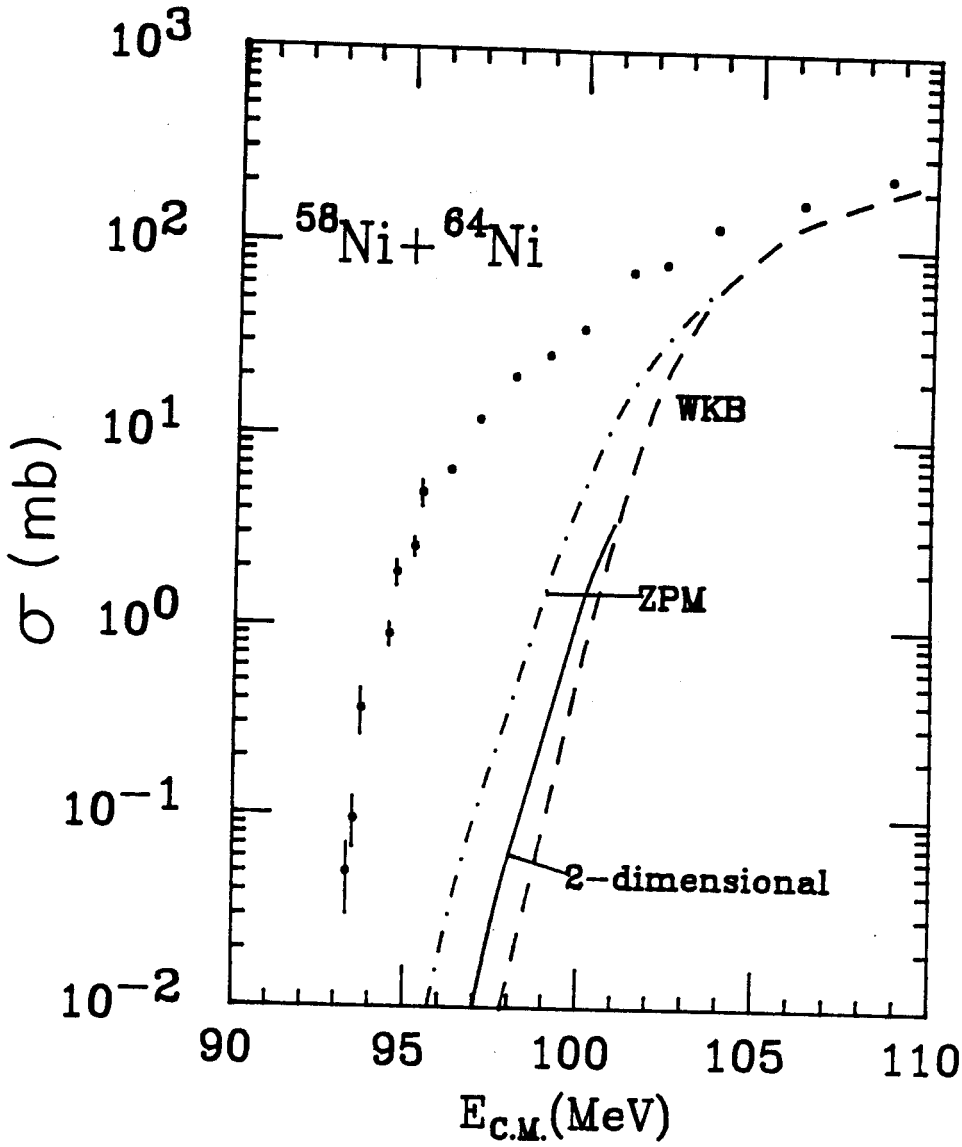

Fig.3.1. Effect of both target and projetile zero-point motion and average dynamical deformation (Coulomb excitation) on the fusion cross section for $^{58}Ni+^{58}Ni \rightarrow ^{116}Ba$. The solid circles give the experimental data of Becherman et al.(Bec.80), the dashed curve gives the result for a one-dimensional barrier corresponding to spherical nuclei, and the solid curv gives final result for a two-dimensional potential-energy surface, and the dot-dashed curve gives the result of ZPM without dynamical deformation.

systems which will be studied in chapter 5 one can ignore Coulomb excitation.

Now we discuss the effect due to angular momentum transfer. In general, there is an angular momentum transfer between intrinsic degrees of freedom and the relative motion when one of or both of the nuclei are excited during the collision in a fusion reaction. For a total angular momentum J, there are several different orbital angular momenta possible. The radial wave function of the relative motion in a channel therefore can be labeled as $R_{n;}(r)_{J,\ell,s_n}$, where n denotes the nTH excited intrinsic state(s), ℓ the orbital angular momentum, s_n the intrinsic spin coupled with ℓ to J. For a fixed n and J, R(r) are different for different ℓ's. The differences come from the term $\frac{\hbar^2\ell(\ell+1)}{2M\ r^2}$ in the Hamiltonian which governs the radial motion. However, in heavy ion reactions, the $\frac{\hbar^2}{2M}$ is a small number. For example, for $^{50}Ti+^{90}Zr$, the $\frac{\hbar^2}{2Mr^2}$ at the Coulomb barrier is only about 6 KeV. So the differences in $\frac{\hbar^2\ell(\ell+1)}{2\ M\ r^2}$ for ℓ's coupled with s to J are negligible. Thus the Hamiltonians for a definite J and n are approximately same. In subbarrier fusion reactions, the different ℓ's coupled with s to J don't have any significance as far as the final product (compound nucleus) is concerned. One would like to reduce the number of channels by not distinguishing different ℓ's and the orientations of intrinsic spin for same n and J, i.e., label a channel by n and J only. If this is possible, the number of channels will be greatly reduced. For instance, for s=2 and $J \geq 2$, the original 25 channels is reduced to a single channel.

We follow Takigawa (Tak.85) to show that it is possible. We consider a system of two even-even nuclei, where either the projectile or the target has one- and two-phonon states of a vibrational mode of excitation with multipolarity λ. We denote the wave function of the relative motion in the entrance channel as $\chi^0_J(r)$, J being the initial angular momentum. We distinguish the one-phonon channels by the angular momentum ℓ of the relative motion, and the two-phonon channels by the total intrinsic angular momentum Λ in addition. Accordingly, we denote the wave function of the relative motion in a one-phonon channel and in two-phonon channel by $\chi^1_\ell(r)$ and $\chi^2_{L\Lambda}(r)$, respectively. The coupled channel equations become

$$\left(-\frac{\hbar^2}{2M}\frac{d^2}{dr^2} + U(r) + \frac{\hbar^2 J(J+1)}{2M\,r^2} - E\right)\chi^0_J(r) + f(r)\sum_\ell N_\ell \chi^1_\ell(r) = 0 \qquad (3.21)$$

$$\left(-\frac{\hbar^2}{2M}\frac{d^2}{dr^2} + U(r) + \frac{\hbar^2 J(J+1)}{2M\,r^2} - E - \hbar\omega\right)\chi^1_\ell(r) + f(r)\,N_\ell \chi^0_J(r) + \sqrt{2}\,f(r)\sum_{L,\Lambda} M^\ell_{L\Lambda}\chi^2_{L\Lambda}(r) = 0 \qquad (3.22)$$

and

$$\left(-\frac{\hbar^2}{2M}\frac{d^2}{dr^2} + U(r) + \frac{\hbar^2 J(J+1)}{2M\,r^2} - E - 2\hbar\omega\right)\chi^2_{L\Lambda}(r) + \sqrt{2}\,f(r)\sum_\ell M^\ell_{L\Lambda}\chi^1_\ell(r) = 0\,, \qquad (3.23)$$

where $N_\ell = \sqrt{(2\lambda+1)/4\pi}\,\sqrt{(2\ell+1)/(2J+1)}$ (3.24)

and

$$M^\ell_{L\Lambda} = (-1)^{J-L-\lambda}\sqrt{(2\ell+1)(2\Lambda+1)(2\lambda+1)/4\pi}\,\langle\lambda\ell 00|L0\rangle\,\begin{Bmatrix}\ell & \lambda & J\\ \Lambda & L & \lambda\end{Bmatrix}. \qquad (3.25)$$

Here, $\hbar\omega$ is the phonon energy and $f(r)$ is the coupling form factor. The couplings are assumed to be linear in the coordinate of the vibrational mode of excitation. Also, the change in the centrifugal potential has been ignored.

Now let

$$\bar{\chi}^1(r) = \frac{1}{N} \sum_{\ell} N_\ell \chi^1_\ell(r) \tag{3.26}$$

$$\bar{\chi}^2 \quad (r) = \frac{1}{N^2} \sum_{\ell, L, \Lambda} N_\ell M^\ell_{L\Lambda} \chi^2_{L\Lambda}(r) \tag{3.27}$$

and use the sum rule for three-j and Clebsch-Gorden coefficients. Then we have

$$\left\{D(r) + F(r)\begin{pmatrix} 0 & 1 & 0 \\ 1 & 0 & \sqrt{2} \\ 0 & \sqrt{2} & 0 \end{pmatrix} - \begin{pmatrix} E & 0 & 0 \\ 0 & E-\hbar\omega & 0 \\ 0 & 0 & E-2\hbar\omega \end{pmatrix}\right\} \begin{pmatrix} \bar{\chi}^0 \\ \bar{\chi}^1 \\ \bar{\chi}^2 \end{pmatrix} = 0, \tag{3.28}$$

where $D(r) = -\frac{\hbar^2}{2M}\frac{d^2}{dr^2} + U(r) + \frac{h^2 J(J+1)}{2M\, r^2}$

and $F(r) = \sqrt{(2\lambda+1)/4\pi}\, f(r)$

We now see that the number of channels has been reduced to 3, from 13 for $\lambda=2$ and $J \geq 2$, for example.

Chapter 4 Validity of ZPM and Simple Approximations

In ZPM the intrinsic excitation energy is assumed to be zero. The two-dimensional equation in ZPM can easily be solved numerically. But in general, ZPM tends to overestimate the subbarrier fusion cross section. Because the barrier penetrability is very sensitive to the energy, one would expect ZPM to overestimates subbarrier fusion cross section considerably. In sec.4.1, we will study the validity of ZPM through a numerical example using the coupled-channel method described in chapter 3. Approximations used to combine two independent intrinsic excitation modes into a single one are discussed in sec.4.2. Factorization of the subbarrier fusion enhancement factors due to each individual intrinsic excitation mode is studied in sec.4.3.

4.1 Validity of ZPM

We take the reaction $^{16}O+^{148}Sm$ for head on collisions ($\ell=0$) as an example to see the effects of finite excitations.

The fusion probability is shown in Fig.4.1 as function of the c. m. energy. The calculations are carried out using the direct matrix inversion method described in the previous chapter. The $\hbar\omega=0$ and $\hbar\omega=\infty$ limits are shown together with the results for $\hbar\omega=1$ MeV and 10 MeV. The value of σ was o.27fm, which is close to the value obtained both for the low-lying quadruploe and octupole states in ^{148}Sm. Since the excitation energy $\hbar\omega$ for these states are 0.55 MeV and 1.16 Mev, respectively, we can conclude that the dynamical effect due to the finite value of $\hbar\omega$ will not lead to a major reduction of the subbarrier fusion cross

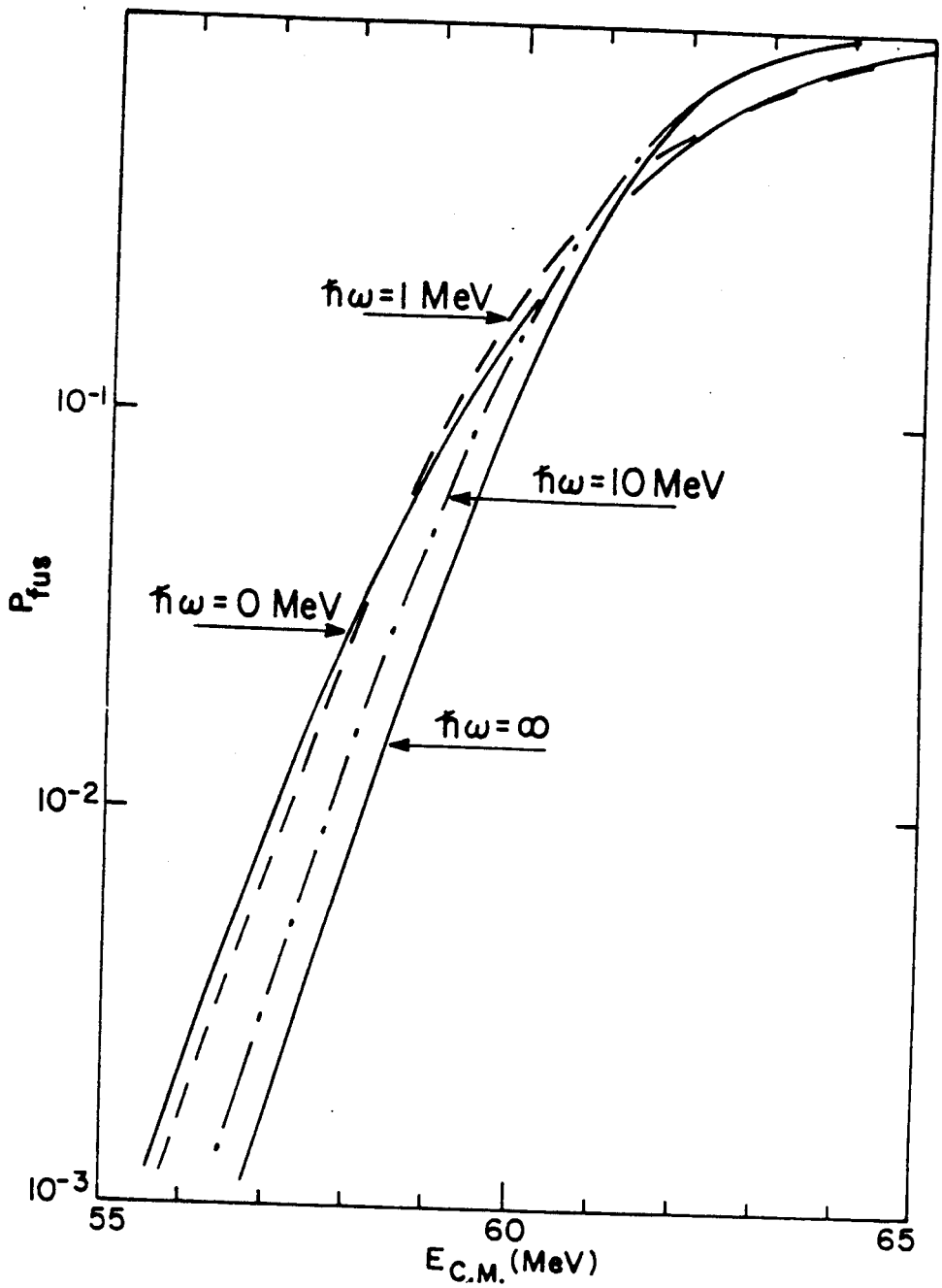

Fig.4.1. Fusion probabilities for the reaction $^{16}O+^{148}Sm$ are shown as function of the c.m. energy. The results are obtained from coupled-channel calculations, for various values of the one-phonon excitation energy $\hbar\omega$. The standard deviation of the zero-point motion amplitude is σ = 0.27 fm.

sections shown in sec.2.3. We see that ZPM is a good approximation when $\hbar\omega$ = 1 MeV in this example.

4.2 Two Independent Degenerate Harmonic Oscillators

In some fusion reactions, more than one intrinsic mode may be coupled to the relative motion. In such cases, the collective coordinates r and s will not be enough to describe the system. Thus the Schrödinger equation has more than two variables, and is numerically very difficult to solve. If one expands the wave function in all intrinsic eigenfunctions, one would find a multidimensional matrix differential equation.

In Ref. (Wu.86) two independent degenerate harmonic vibrations have been combined into one to calculate the fusion cross section. For two modes with same $\hbar\omega$, the σ for the combined mode is given by

$$\sigma = \sqrt{\sigma_1^2 + \sigma_2^2}, \tag{4.1}$$

where σ_1 and σ_2 are the r. m. s. amplitudes for each mode, respectively. We discuss this approximation in this section.

The energy spectrum of the combined mode is identical to the original two. But transitions between states are different. First, we show that transition matrix elements from the ground state to excited states are same. The probability of the transition from the ground-state to the n^{th} excited state is proportional to

$$\sum_{i=0}^{n} |\langle 0,0|(s_1+s_2)^n|i,n-i\rangle|^2 = \sum_{j=0}^{n} (C_j^n)^2 \frac{j!}{2^j} \frac{(n-j)}{2^{n-j}} \sigma_1^{2j} \sigma_2^{2(n-j)} 2^j 2^{n-j}$$

$$= \frac{n!}{2^n} (2\sigma_1^2 + 2\sigma_2^2)^n = \frac{n!}{2^n} (2\sigma^2)^n, \qquad (4.2)$$

and is the same as that in a single mode with σ given by eq.(4.1). If one neglect the contributions from higher multipoles in $(s_1+ s_2)$, the combined mode gives same transition rate for the ground state as that given by the two independent modes. However, the transitions between excited states are different. For example, $|\langle 1|s|2\rangle|^2$ in the combined mode is $2\sigma^2 = 2(\sigma_1^2+\sigma_2^2)$, while the original two independent modes gives

$$\frac{1}{2} \{(\langle 0,1|(s_1+s_2)|0,2\rangle)^2 + (\langle 0,1|(s_1+s_2)|1,1\rangle)^2 +$$

$$(\langle 1,0|(s_1+s_2)|2,0\rangle)^2 + (\langle 1,0|(s_1+s_2)|1,1\rangle)^2 = \frac{3}{4} 2(\sigma_1^2 + \sigma_2^2), \qquad (4.3)$$

where the factor of $\frac{1}{2}$ represents an averaging over the initial states.

In Fig.4.2, we show the numerical results for $^{50}Ti+^{90}Zr$, the coupling parameters given in Table 4.1 are arbitrary, and for the

Table 4.1. Parameters used in obtaining Fig.4.2 and Fig.4.3.

System	V_0	a	ΔR	σ_1	σ_2	σ	$\hbar\omega_1$	$\hbar\omega_2$	$\hbar\omega$
$^{50}Ti+^{90}Zr$	-31.7MeV	0.63fm	0.35fm	0.2fm	0.2fm	0.28fm	1.5MeV	1.5Mev	1.5Mev

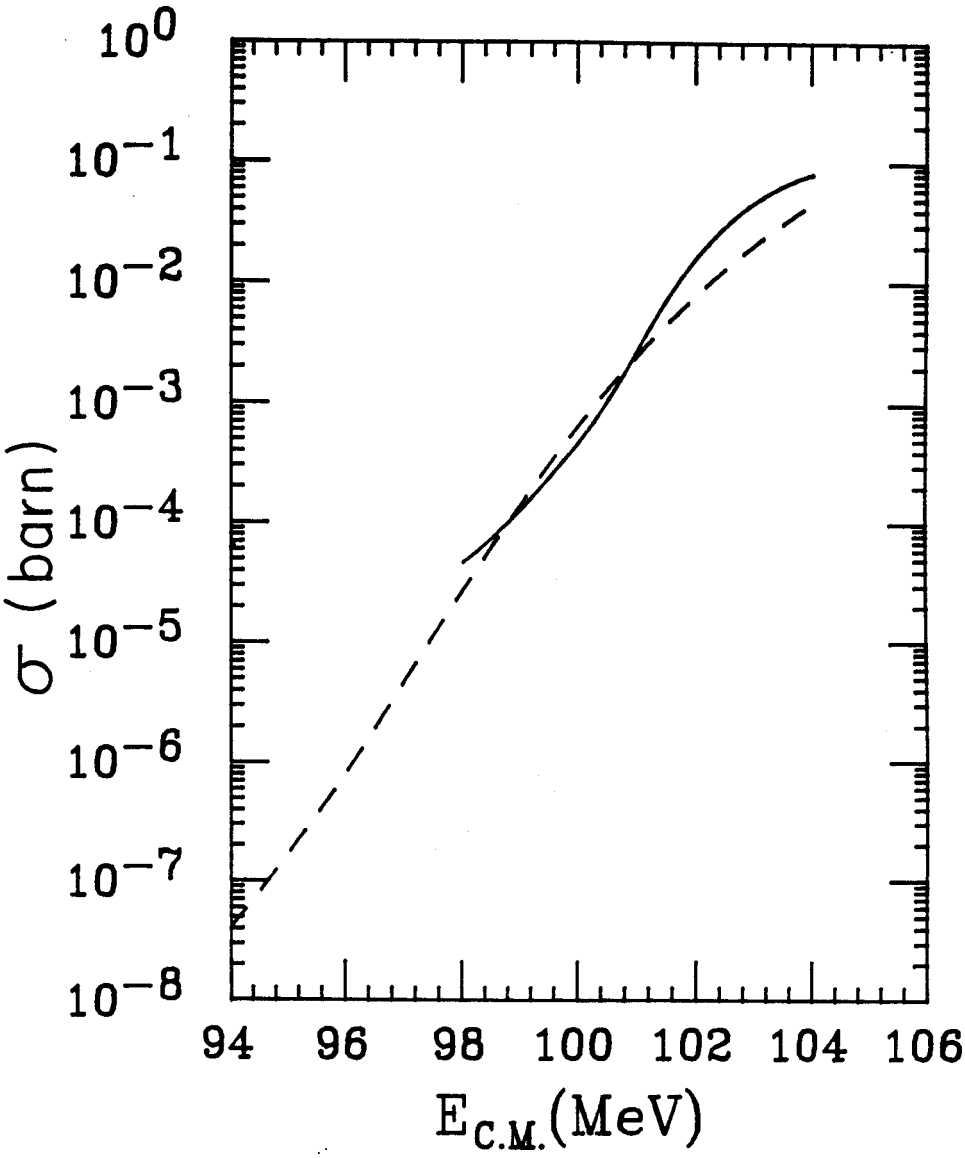

Fig.4.2. S-wave fusion excitation function is shown as function of c.m. energy. The dashed curve is the result obtained by combining two vibrational modes into single one through eq.(4.1). The solid line is the result obtained by solving exactly a three-dimensional coupled equation. Due to numerical restrictions, the exact result can not be obtained for enrgies lower than 98 MeV. The parameters used are given in Table 4.1.

purpose of comparison only. The combined mode gives the same results as that given by a three-dimensional calculation. The three-dimensional calculation in which two independent vibrations are simultaneously coupled to the relative motion is very difficult and time consuming, and can not be calculated for even lower energies.

4.3 Factorization of The Enhancement Factors

When several modes of intrinsic excitations are coupled to the relative motion in a fusion reaction, the subbarrier fusion enhancement over the conventional one-dimensional barrier penetration can be quite large. In general, the calculation is very difficult, and it would be nice if the total enhancement factor could be given by the product of the enhancement factors obtained by coupling only one mode at a time. If this were true, instead of doing a multidimensional penetration calculation, one would only have to solve a number of two-dimensional problems. Certainly this is not true for energies just below the barrier, because the transmission probability can not exceed 1, while the product of the enhancement factors may give a transmission probability greater than 1. The same argument does not have to be true for energies far below the barrier.

In Fig.4.3, we show the enhancement factors as functions of energy in the center of mass frame. The total enhancement factors (solid curve) is obtained by using eq.(4.1) to combine two identical vibrations into a single one. The parameters used in the calculations are also given in Table 4.1. The σ's and $\hbar\omega$'s are arbitrary, but close to the

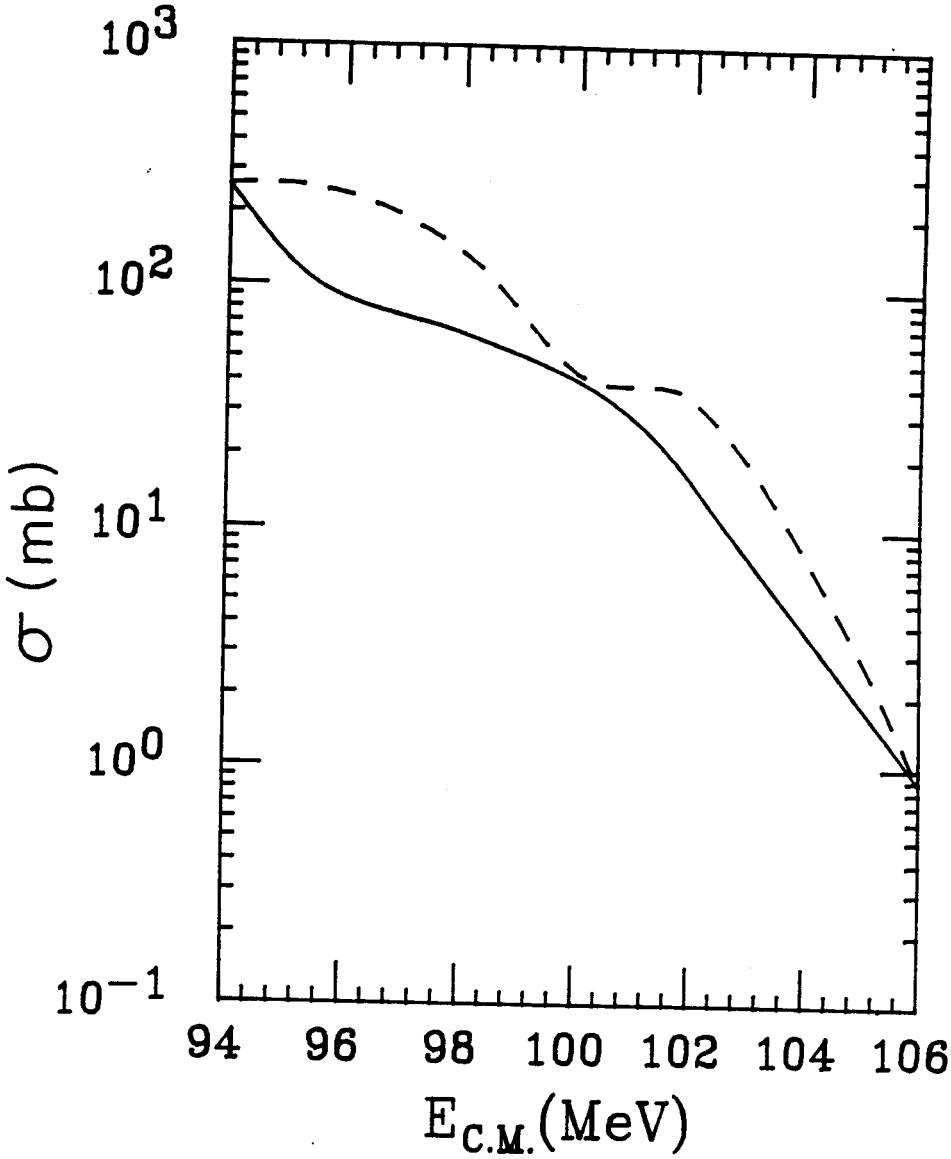

Fig.4.3. Fusion enhancement factors are shown as functions of c.m. energy. The solid line is the result obtained by combining two vibrational modes into one through eq.(4.1). The dashed curve is the result obtained by virtue of factorization rule. The parameters used are listed in Table 4.1.

actual values. They were assigned for the purpose of discussion only. The product of the two enhancement factors (taken to be same here) is persistently larger than the calculated total enhancement factor. Therefore one can use the factorization rule only to estimate the upper limit of the enhancement.

Chapter 5 Subbarrier Fusion in Light Nuclei

In this and next two chapters, we study subbarrier fusion in various systems. The systems treated in this chapter are $^{16}O+^{16},^{18}O$. Since, in general, a realistic coupled channel calculation is numerically difficult, it is important to find simpler cases which are more amenable to a complete theoretical treatment. The study comparing fusion cross sections of ^{18}O and ^{16}O on ^{16}O targets provides a nice case that can be treated without much ambiguity in a model. Therefore, it provides a nice test for the model.

For $^{16}O+^{16}O$ system, the internal degrees of freedom are relatively unimportant because of the high excitation energies of the inelastic channels and particle transfer channels. The nucleus ^{18}O on the other hand has a 2^+ state at 1.98 Mev excitation with a transition strength 16.6 of Weisskopf units from the ground state.

The experiment findings (Tho.85) is that the ^{18}O fusion cross section is enhanced over ^{16}O in the subbarrier region. We show this in Fig.5.2 with the cross section ratio plotted as a function of the c. m. energy. The enhancement is small compared to that found in heavier systems, but there is certainly an effect present. In ref. (Tho.85), it is suggested that the difference is mainly due to the changes in the potential barrier going from one system to another. Therefore, as a first step in the analysis, we will examine the expected effect on the potential by adding two neutrons to ^{16}O. We also expect a significant effect from the low-lying 2^+ state, which may be roughly estimated with the frozen approximation mentioned in cnapter 2. According to eq.(24)

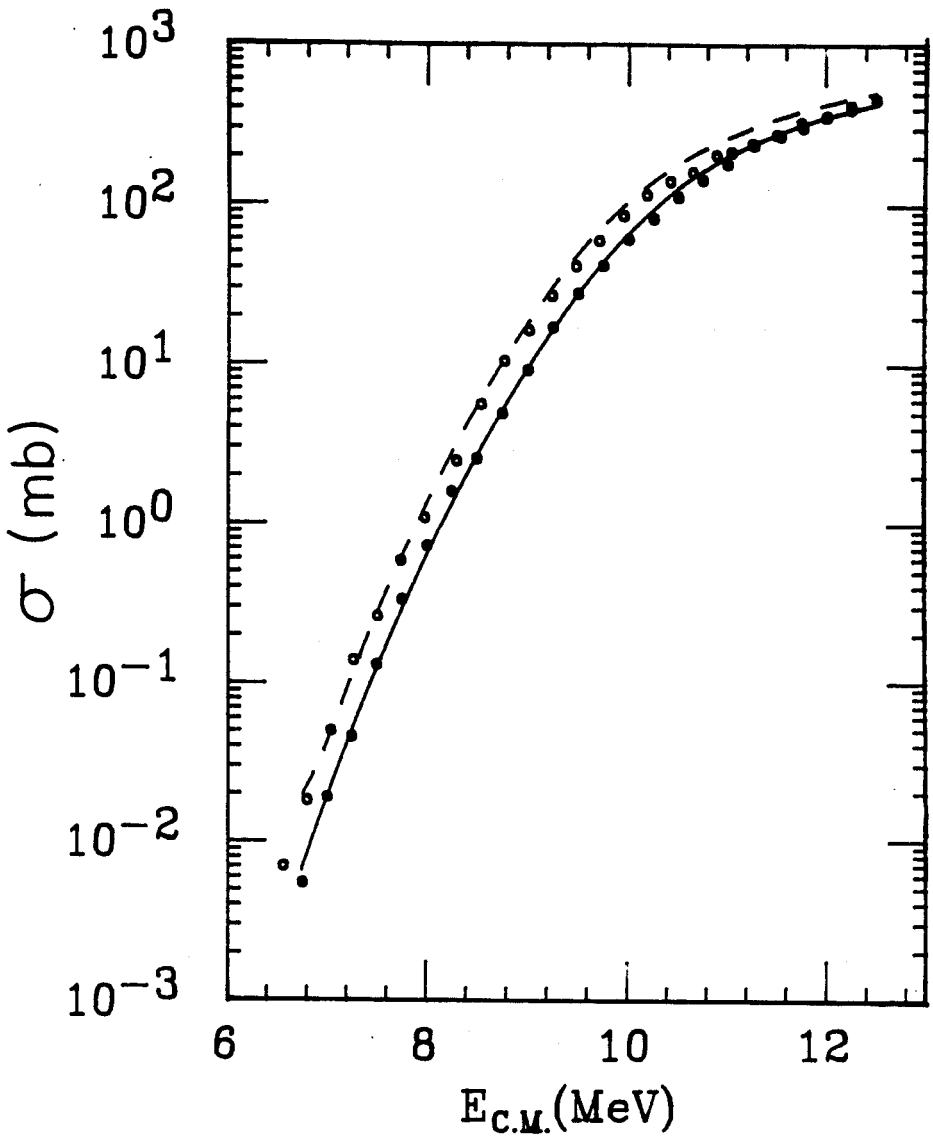

Fig.5.1 The measured fusion cross section for $^{18}O+^{16}O$ and $^{16}O+^{16}O$, from ref. (Tho.85) is shown by the experimental points. The potential model fit to the $^{16}O+^{16}O$ is shown as the solid line, and the coupled-channel model with rescaled potential is shown by the dashed line.

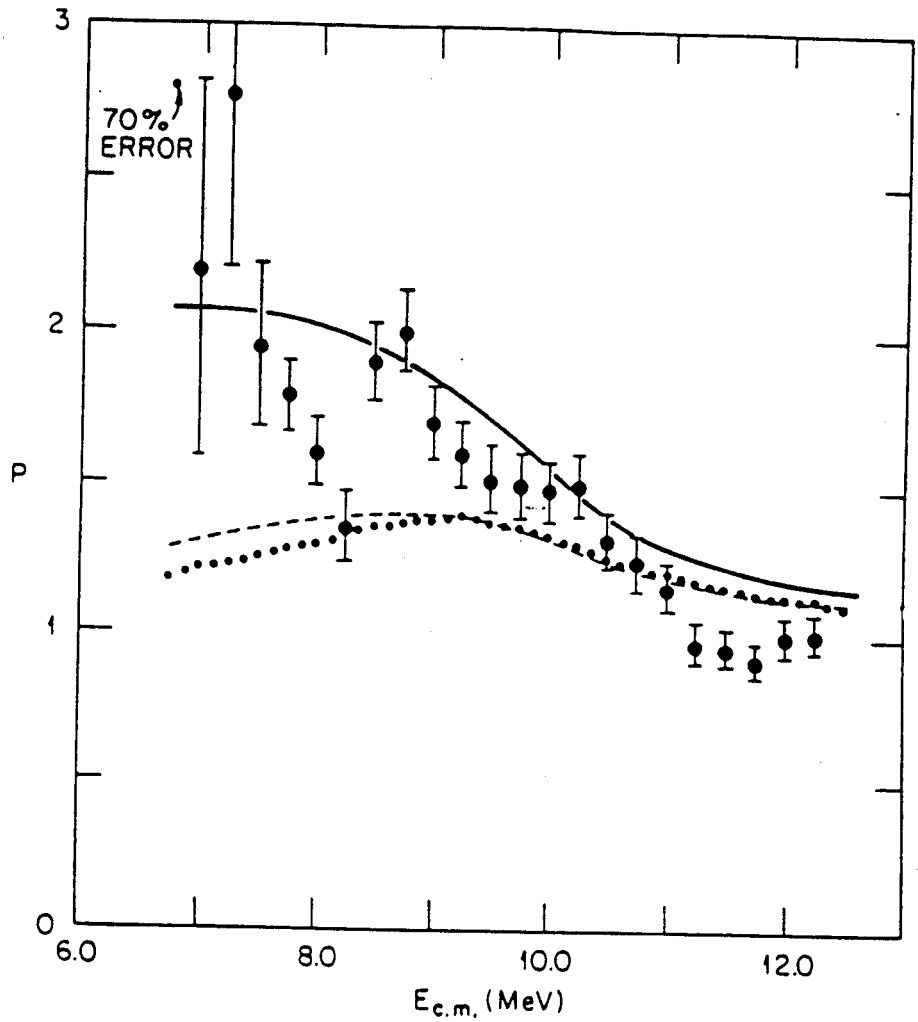

Fig. 5.2. Enhancement factors extracted by log-linear interpolation of the data from ref. (Tho.85). The dashed line is the prediction of the rescaled potential, eq.(3.2). The dotted line is the prediction of the potential eq.(5.3). The solid line is the prediction of the coupled-channel model with the rescaled potential.

in ref. (Esb.83), the enhancement in the subbarrier fusion may be estimated as

$$P=\left[\frac{1}{2}\left(\frac{2\pi Z_1 Z_2 e^2}{\hbar\omega_0 R_b^2}\,\sigma\right)^2\right], \tag{5.1}$$

where R_b is the position of the Coulomb barrier and $\hbar\omega_0 = \left.\frac{\partial^2 V}{Mr^2}\right|_{r=R_b}$. The constants in the above expression may be estimated as follows for the $^{18}O+^{16}O$ system. The deformation length associated with the $0^+ - 2^+$ transition is determined from the transition strength by eq.(2.7). This yields a value $\sigma = 0.33$ fm. From the potential model fit to the barrier described below, we find a barrier height of 9.7 MeV at a radius $R_b = 8.9$ fm. The thickness of the barrier at an energy of 6.75 Mev is 6 fm, which corresponds a parabolic barrier having an oscillator frequency of $\hbar\omega = 1.8$ MeV. The predicted enhancement with these parameters is 2.5, indicating that the excited state in ^{18}O may significantly effect subbarrier fusion.

The detailed calculations employ the coupled channel technique described in chapter 3 to calculate the fusion cross section. The potential in each channel is purely real, and an incoming wave boundary condition is imposed at a small radius, which we take to be 4.1 fm. The coupled channel equations are solved by the direct matrix-inversion method, which is much more reliable than iterative techniques for energies below the barrier. As in chapter 3 we use the internuclear potential of eq.(3.2), dropping the quadrupole Coulomb field. The two nuclear radii R_1 and R_2 are determined by eq.(3.3). We found that the

potential fits the fusion data of $^{16}O+^{16}O$ quite well with the parameter set

$V_o = -39.8$ Mev/fm, $\Delta R = 0.45$ fm, and $a = 1.65$ fm. Since the potential is of the proximity form, we can extrapolate to an $^{18}O+^{16}O$ potential changing one of the radii according to eq.(3.3). The rescaled potential is wider and deeper than the original ^{16}O potential, giving more subbarrier fusion. However, the enhancement is rather small, as may seen by the dashed line in Fig.5.2. Of course, the proximity scaling may not be a reliable way to extrapolate the influence of the valence neutrons on the potential, so we also examined their effect in a folding model. Namely, we determined the $^{18}O+^{16}O$ potential according to

$$V(^{18}O+^{16}O) = V(^{16}O+^{16}O) + \int \rho(r')\, U(r-r')\, d^3r'. \qquad (5.2)$$

Here $U(r)$ is a Woods-Saxon potential with parameters given in ref. (Boh.69), and ρ is the valence neutron density determined from the d-wave bound state in that Woods-Saxon potential. This method also gives a small enhancement, which is shown by the dotted line in Fig.5.2. Thus, we are inclined to reject the potential barrier variation as the main mechanism for producing the ^{18}O enhancement.

The potential matrix for the coupled channel calculation is constructed by a macroscopic model of the excitation. We assume the 2^+ state to be a harmonic vibration of the surface deformation coordinate s, and evaluate the matrix elements according to eq.(3.8), which yields,

$$\tilde{V} = \begin{vmatrix} \langle 0|V_n(r-s)|0\rangle + V_c & \langle 0|V_n(r-s)|1\rangle \\ \langle 0|V_n(r-s)|1\rangle & \langle 1|V_n(r-s)|1\rangle + V_c + 1.98 \end{vmatrix} \qquad (5.3)$$

In this equation, we have neglected the angular momentum transfer, an effect treating the combined system in a rotating frame approximation. The integral over s is easily performed for the error function, giving

$$\langle 0|V_n(r-s)|0\rangle = V_n(r)|_{a'=(a^2+2\sigma^2)^{1/2}}$$

$$\langle 1|V_n(r-s)|0\rangle = \sigma \frac{d}{dr}\langle 0|V_n(r-s)|0\rangle. \qquad (5.4)$$

The wave function for each entrance channel angular momentum is found by integrating the coupled equations out from the inner boundary. For the energies we study here, the sum over angular momentum can be truncated at ℓ=12, with an accuracy of 1%. The predicted enhancement including the potential and coupled channel effects is shown as the solid curve in Fig.5.2. As expected from the frozen approximation, the inclusion of channel coupling substantially enhances the cross section in the subbarrier region. However at energies above the barrier, the theory predicts the enhancement to persist, while experimentally equal cross section are found. We will return to this later.

The coupled-channel model of eq.(5.3) is oversimplified in several aspects, and the assumptions need to be examined and justified. First the higher excitations in ^{18}O might increase the cross section even more. In fact, such couplings are implicit in the harmonic model used to derive the sudden approximation, eq.(5.1). However, the B(E2) from the first 2^+ state to the triplet states near 4 MeV is lower than that from the ground-state to the first 2^+ state, while the harmonic model require a larger B(E2). We find that including these channels in a five-dimensional matrix has a negligible effect on the fusion cross

section. Another oversimplification in the model is the neglect of the Coulomb excitation of the 2^+ state. It is shown in chapter 3 that for medium heavy systems the Coulomb part of the Coupling interferes destructively with the nuclear part and reduces the subbarrier enhancement. Indeed, we find that by including Coulomb excitation according to eq.(3.2), the cross section is reduced by as much as 7% at the lowest energy, becoming less important as the energy goes up. As mentioned above, the coupled-channel model treats the system in a rotating-frame approximation. The physical justification for this is that we expect axially symmetric deformations to provide the dominant path for fusion. The angular momentum transfer assumption was tested with the code PTOLEMY, used to compare the cross sections treating the excited state as L=2 or L=0. The cross section at subbarrier energies comes out larger with angular momentum transfer, by an amount comparable to the Coulomb correction. Since both effects are small and opposite in sign, we are justified in neglecting them in this context. Nucleon transfer effects are also not included in the formalism. One might expect that the two neutron transfer, which has a zero Q-value, plays a dominant role. However, for such processes, contributions in the even and odd partial waves have opposite signs and cancel in the Q = 0 limit.

Above the barrier, the cross section is reduced by the angular momentum transfer, but not enough to equalize the cross sections of the two reactions. The experimental observation of equal cross sections is inexplicable. A channel coupling under the barrier will always enhance the cross section. For the low-partial waves that go over the barrier, it is hard to see how the extra couplings in the $^{18}O+^{16}O$ system could reduce the transmission factor. It appears to be a general phenomenon

found also for other systems that the fusion cross sections above the barrier come out too large when the model is fit to subbarrier fusion data. We will see some of examples of this later.

Chapter 6 Subbarrier Fusion in Medium Heavy Nuclei

For heavy systems, one has to go beyond the potential barrier model to reproduce the data. This was convincingly demonstrated in work by Balantekin et al. (Bal.83), in which an effective one-dimensional potential was extracted directly from the fusion data. Fig.6.1 shows the extracted potential for various systems, from light to medium heavy. For the ^{74}Ge+^{64}Ni system one finds a barrier whose inner edge has an unphysical negative slope. Thus, one cannot fit with the data by manipulating the parameters or forms of one-dimensional potentials. In this chapter, a quantitative treatment of subbarrier fusion extending to heavy nuclei is presented. The systems studied are Ti, Br + Zr, Nb and Zr+Zr. In the following section we discuss the parameters of the calculations, and the results are presented in sec.6.2.

6.1 Details of The Calculations

The formulation of the surface-coupling model follows that given in sec.3.1. The internal degrees of freedom are described by a harmonic-oscillator Hamiltonian with an internal coordinate s. The coupling to the radial coordinate is through the ion-ion potential, and is given by eq.(3.2). The parameters V_0, R_i, and a are given by eq.(3.3). For the systems Ti+Zr and Ti+Nb, ΔR was adjusted to reproduce the experimental fusion cross sections in the barrier region for ^{50}Ti+^{90}Zr and ^{46}Ti+^{93}Nb using the one-dimensional model, respectively. For Br+Zr systems, we fit the subbarrier fusion data of ^{81}Br+^{90}Zr to determine ΔR and σ in ^{81}Br for this isotopic system. The parameter ΔR is found to be

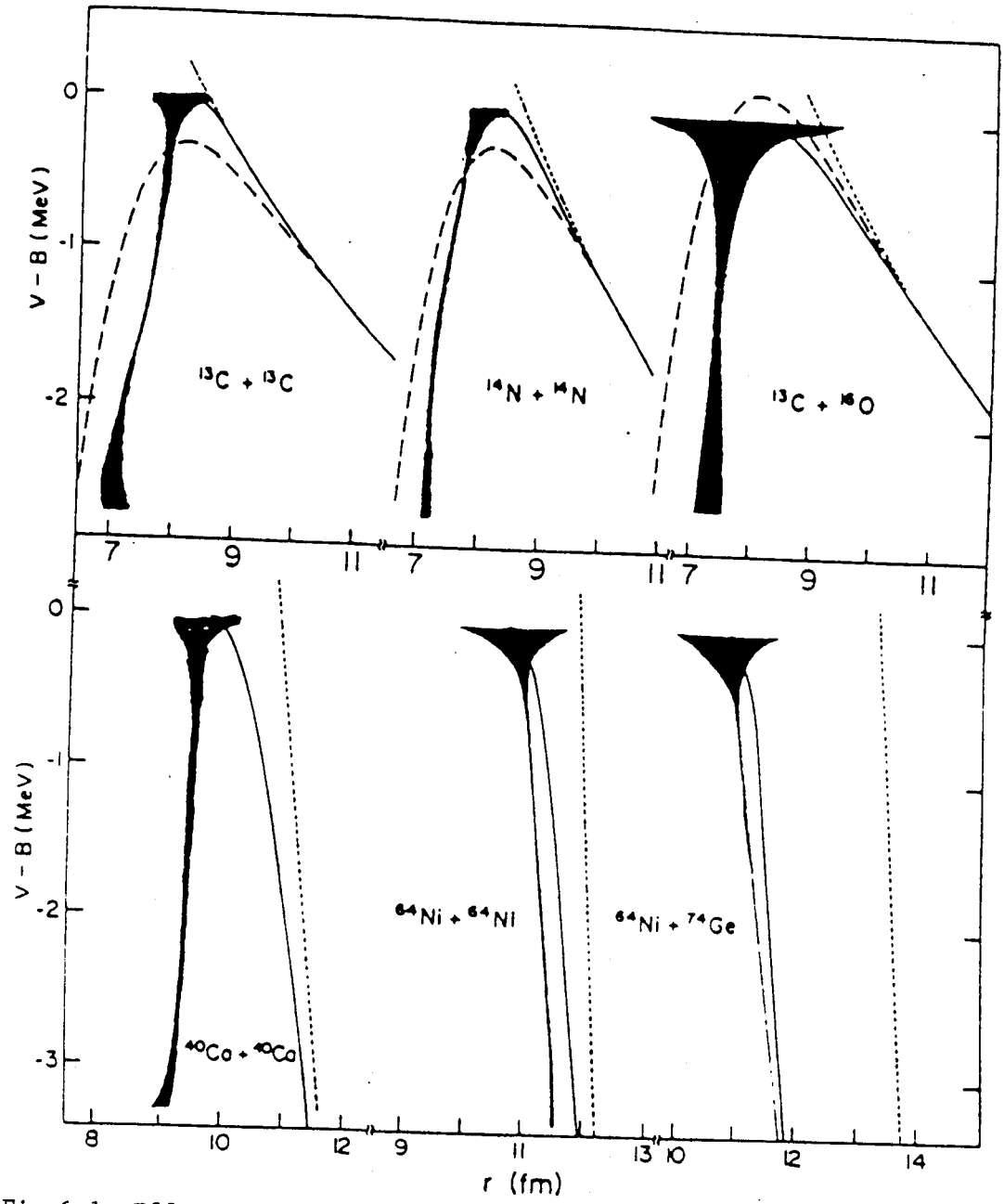

Fig.6.1. Effective one-dimensional potential barriers for $^{13}C+^{13}C$, $^{14}N+^{14}N$, $^{13}C+^{16}O$, $^{40}Ca+^{40}Ca$, $^{64}Ni+^{64}Ni$, and $^{64}Ni+^{74}Ge$. The outer turning point is determined from the KNS potential readjusted as described in ref. (Bal.83) to fit the peak positions. The thickness is inverted from fusion cross sections and the shaded region indicates the error. The short dashed line denotes the point Coulomb potential, the long dashed curves in the upper figures denote the unmodified KNS potential, and for ease of presentation the energy is plotted relative to the barrier height.

0.35 fm for Ti+Zr systems and 0.40 fm for all other systems. It should be mentioned that these parameters are far from unique as far as fusion is concerned. At most two parameters are determined by the above-barrier cross section, namely the barrier height and the barrier position. Other sets of V_o, a and ΔR give the same fit and the same coupled channel results below the barrier.

The intrinsic oscillator Hamiltonian $H_{in}(s)$ is specified by the frequency $\hbar\omega$ and by σ, the r.m.s. amplitude of the coordinate in the ground state. The coupled-channel equation for the system is therefore given by eq.(3.6). The internal Hamiltonian $H_{in}(s)$ should be chosen to reproduce the energy and transition strength of the lowest excitations of the nuclei. For a single nucleus, the relation of σ to the B(EL) of a transition is given by eq.(2.7):

$$\sigma_\lambda = \frac{R}{Z(\lambda+3)} \left((2\lambda+1)\frac{B(E\lambda)}{B_w(E\lambda)}\right)^{\frac{1}{2}}. \qquad (2.7)$$

The excitation of both nuclei may be treated with a single coordinate s, if the energies are degenerate; in that case the effective amplitude of the deformation is related to the individual amplitudes by

$$\sigma = \sqrt{\sigma_1^2+\sigma_2^2} \qquad (4.1)$$

Eq.(4.1) will also be applied in cases where the excitation energies are not degenerate and both excitations are important. The lower of two energies will be used if the difference is small. Otherwise we take the average of two energies as oscillator energy. As

Table 6.1. Parameters of surface vibrations deduced from the measurement of low lying state. For odd nuclei they are averages of those of two neighboring even-even nuclei. The σ's (standard deviations) are calculated according to eq.(2.7).

Nucleus	Energy of the First Excited State (MeV)	s(fm)
^{90}Zr	2.18	0.16
^{94}Zr	0.91	0.16
^{50}Ti	1.55	0.25
^{46}Ti	0.889	0.49
^{81}Br	0.7	0.36
^{93}Nb	0.9	0.22

Table 6.2. Parameters of surface vibrations used in the fusion cross-section calculations of Figs.6.2,3,4,5,6. The parameters in parenthesis were obtained by fitting to the data. The rest were taken or calculated from Table 6.1

Reaction	$\hbar\omega$ (Mev)	σ(fm)
^{50}Ti+^{90}Zr	1.55	$0.3=\sqrt{0.25^2+0.16^2}$
^{46}Ti+^{90}Zr	0.918	(0.39)
^{46}Ti+^{93}Nb	0.9	$0.45=\sqrt{0.22^2+(0.39)^2}$
^{50}Ti+^{93}Nb	$1.2=\frac{1}{2}(0.9+1.5)$	$0.32=\sqrt{0.22^2+0.25^2}$
^{81}Br+^{90}Zr	(0.9)	(0.32)
^{81}Br+^{94}Zr	0.9	$0.36=\sqrt{(0.32)^2+0.16^2}$

we shall see this procedure gives the parameters for H_{in} that describe the reaction $^{50}Ti+^{90}Zr$ very well below the barrier. For the softer system $^{46}Ti+^{90}Zr$, the method gives too much subbarrier fusion and we treat σ as an adjustable parameter.

For an odd nuclei the $\hbar\omega$ and σ of the collective excitation are hard to extract from the data on low-lying states. They are chosen to fit the fusion data for one system and kept same for other systems. We expect the values of these parameters lie between those of two neighboring even-even nuclei. For ^{93}Nb, the averaged parameters σ and $\hbar\omega$ describe subbarrier fusion excitations of $^{50}Ti+^{93}Nb$ and $^{46}Ti+^{93}Nb$ very well.

The coupled-channel calculations were carried out using the direct matrix-inversion method. The inner boundary was chosen at the point where the potential in the entrance channel is the minimum. The results do not sensitively depend on where the boundary is. The internal excitation parameters extracted from experimental data are listed in Table 6.1. Table 6.2 shows the coupling parameters used in the calculations.

6.2 Results and Discussions

The fusion excitation function for $^{50}Ti+^{90}Zr$ calculated from the model is compared with experiment (Ste.85) in Fig.6.2. As one can see, the fusion is underestimated by the conventional barrier penetration model (bold continuous curve), a factor of 60 too low at $E_{c.m}$=100.6 MeV, although they were fit in the barrier region. The fusion is enhanced by

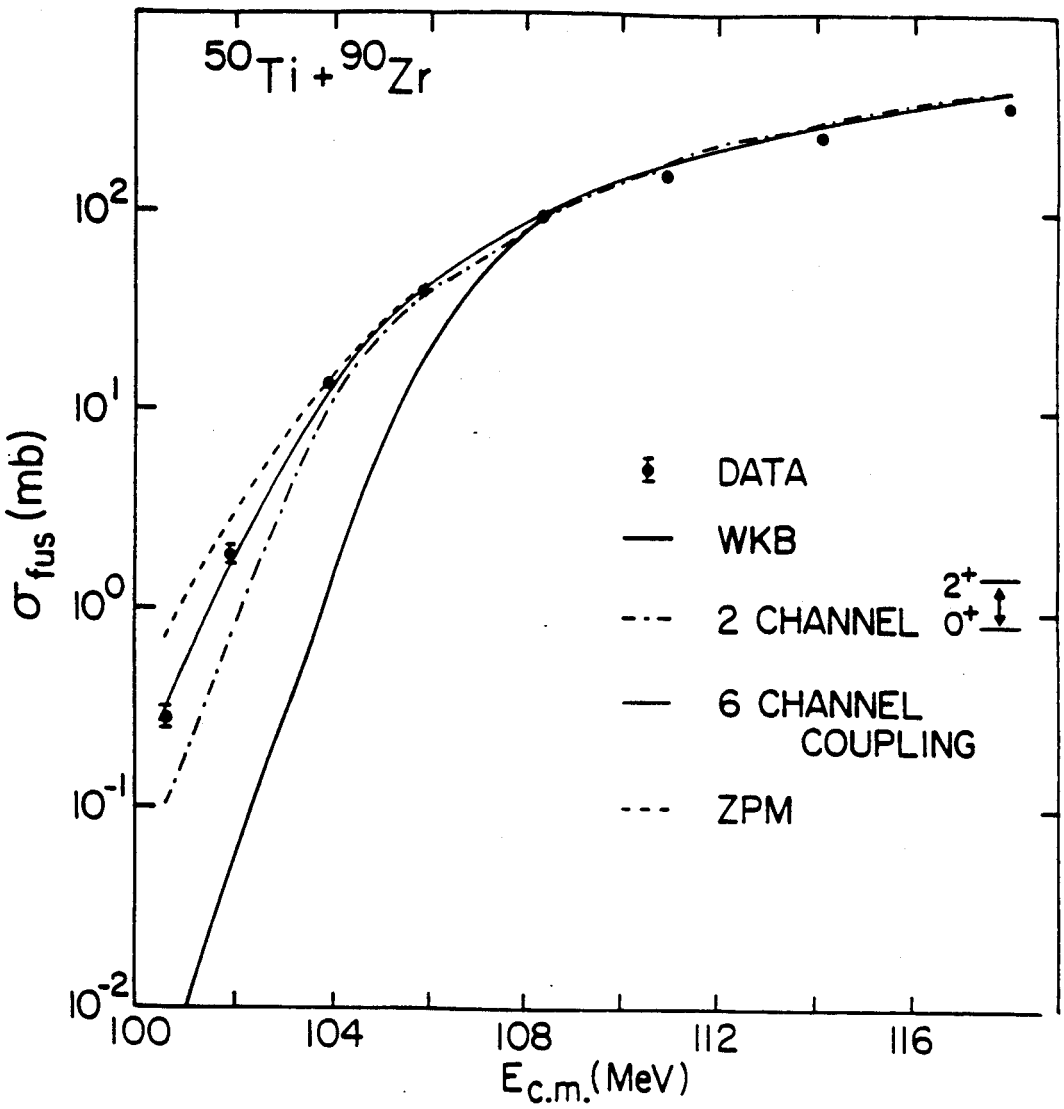

Fig. 6.2. Fusion cross sections for $^{50}Ti+^{90}Zr$. The bold continuous curve is the results of the one-dimensional barrier penetration calculations. The two-channel coupling result is shown by dash-dotted curve. The thin continuous curve is the result obtained by solving 6 channel coupled equation. The 6 channels correspond to the first 6 excited vibrational states assumed in ^{50}Ti with a energy spacing of 1.55 MeV. The dashed curve is the prediction from ZPM. All calculations include the quadrupole Coulomb excitation and ignore the angular momentum transfer.

coupling the excitation of the first excited state to the relative motion (dash-dotted curve). But the fusion is still underestimated by a factor of 3 at the lowest energy. One is naturally led to expect that the contributions from higher intrinsic excitations would account for the difference. But the parameters of couplings of the higher excitations to the relative motion is very hard to extract from the spectrum. However, if one approximate these excitations as pure harmonic vibrations, one would get the full-channel coupling results shown by the thin continuous curve in Fig.6.2. The agreement below the barrier is very good in this approximation. The above-barrier fusion is slightly overpredicted by our model, though the $(Z/A)_{eff}$ of the system does not exceed the extra-push threshold (Nix.77). The prediction from ZPM is also shown. Although the orders of magnitude are right, the ZPM overpredicts the fusion of the $^{50}Ti+^{90}Zr$ for energies far below the Coulomb barrier. Alternatively if the ZPM is fit to the subbarrier data, then the potential barrier is too low at higher energies (Ste.85).

Rhoades-Brown et al. (Rho.84) calculated subbarrier fusion cross sections for various medium heavy systems, using the coupled channel version of the PTOLEMY code, which treats angular momentum algebra exactly. A few low-lying states were coupled to the relative motion with parameters extracted from the low-lying excitation measurements. It was found that the subbarrier fusion was greatly enhanced compared to the one-dimensional penetration approximation, but was still underestimated for energies far below the Coulomb barrier, by orders of magnitude in some systems. From our results for $^{50}Ti+^{90}Zr$, we feel that if higher intrinsic couplings are treated correctly, one can reproduce

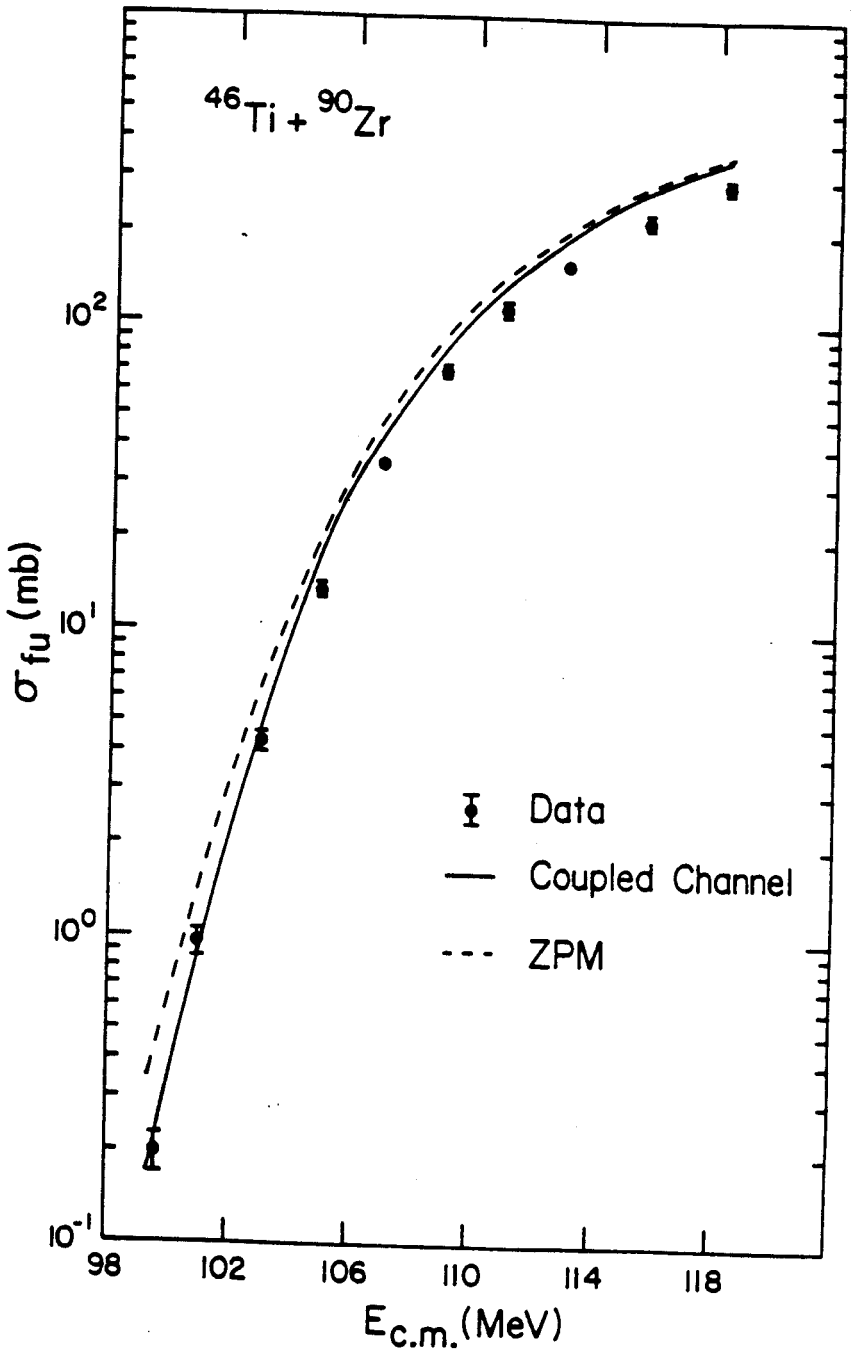

Fig.6.3. Same plot as in Fig.6.2, but for $^{46}Ti+^{90}Zr$. The parameters V_0, Ad, ΔR are kept same as those for $^{50}Ti+^{90}Zr$. 0.89 MeV, the energy of the first excited state in ^{46}Ti, is used as the energy quanta for the vibrational mode. The σ is somehow o.39 fm, different from that quoted from the B(E2) measurement.

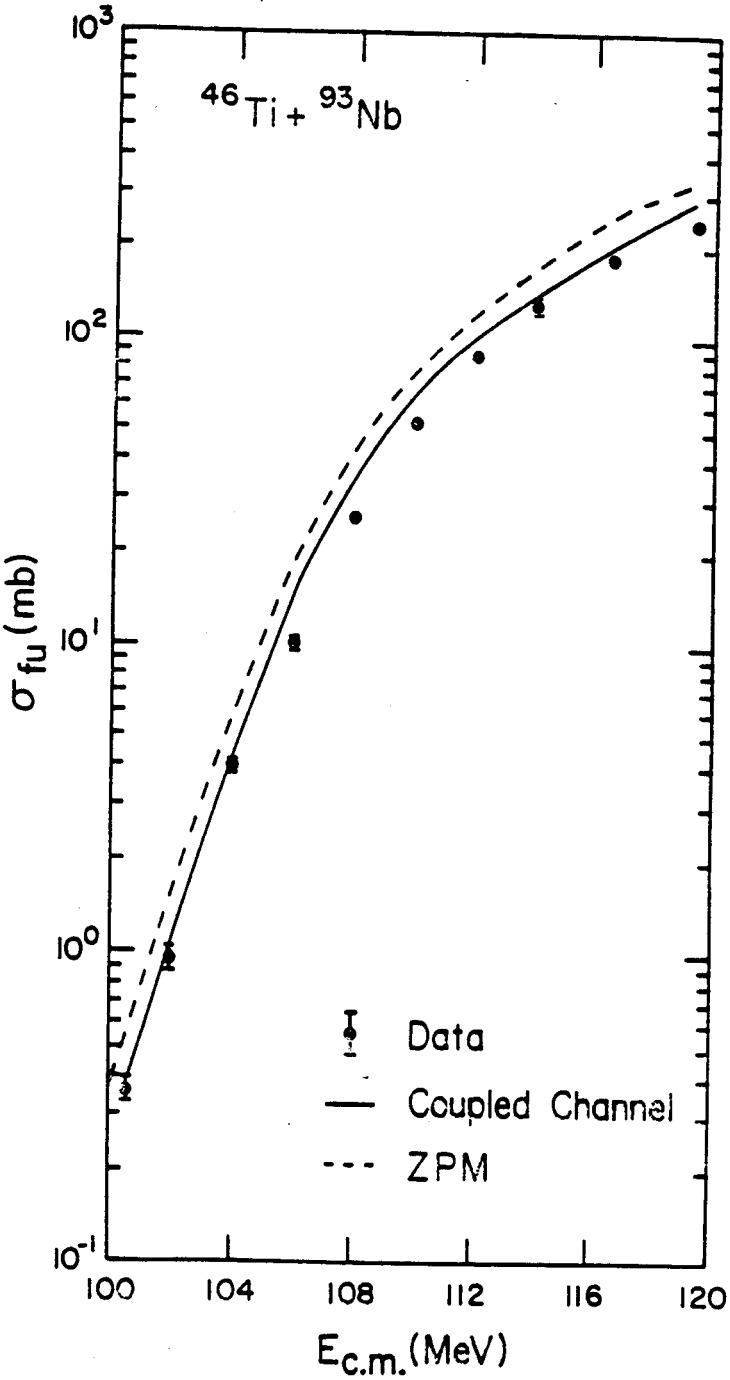

Fig.6.4. Fusion cross sections for $^{46}Ti+^{93}Nb$. The $\hbar\omega$ and σ for ^{93}Nb is taken as the average of those for ^{92}Zr and ^{94}Mo. The excitations in both ^{46}Ti and ^{93}Nb are combined into one mode with $\hbar\omega = \hbar\omega(^{46}Ti) = \hbar\omega(^{93}Nb)$ and the σ equals $\sqrt{\sigma^2(^{46}Ti)+\sigma^2(^{93}Nb)}$. The number of channels coupled is 5.

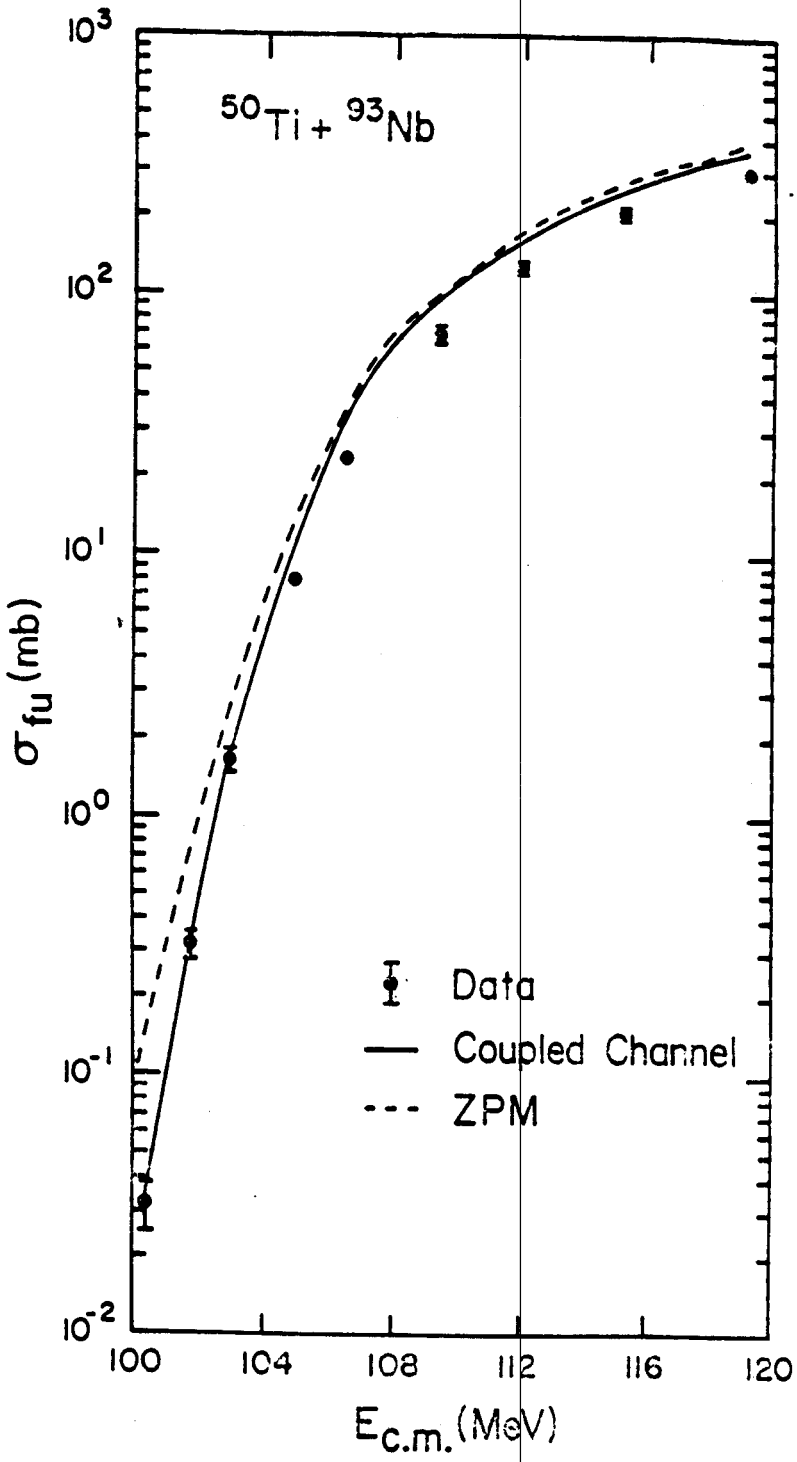

Fig.6.5. Fusion cross sections for $^{50}Ti+^{93}Nb$. In the coupled channel calculation, the $\hbar\omega$ is the average of those for ^{50}Ti and ^{93}Nb. The σ is $\sqrt{\sigma^2(^{50}Ti)+\sigma^2(^{93}Nb)}$.

the data in the coupled-channel model.

In Fig.6.3 we compare the calculation for $^{46}Ti+^{90}Zr$ with the data (Ste.85). Here σ was reduced to achieve agreement with the data. In other words, the subbarrier fusion would be over predicted if we take the experimental value for σ. This suggests that the excitations in ^{46}Ti can not be approximated as pure harmonic vibrations. The ZPM is more successful (closer to the coupled-channel result) for $^{46}Ti+^{90}Zr$ because the excitation energy is lower, only 0.88 MeV. In Fig.6.4 and Fig.6.5 we show the results for $^{46}Ti+^{93}Nb$ and $^{50}Ti+^{93}Nb$. The $\hbar\omega$ and σ for ^{93}Nb were taken as the average of those for ^{92}Zr and ^{94}Kr. Again the agreement is good.

For heavier systems, fusion is inhibited at the configuration just inside the Coulomb barrier (Nix.77, Swi.81). The threshold projectile-target parameters for inhibition is given by (Bir.83)

$$K_{thr} = (Z^2/A)_{eff\ thr} = 35\ \{1-1.78[(N_1-Z_1+N_2-Z_2)/(A_1+A_2)]^2\} \approx 35.$$

The Ti+Zr, Nb systems have $K_{critical} \approx 25$, well below the threshold value.

The next fusion reactions we consider have values of K around the threshold value in s-wave channel. The systems we consider are $^{81}Br+^{90,94}Zr$, and $^{90}Zr+^{90\ 94}Zr$, measured by Beckerman et al. (Bec.84). In Fig.6.6 we plot the fusion cross section ratio of the $^{81}Br+^{94}Zr$ to the $^{81}Br+^{90}Zr$. The effects of ^{90}Zr excitation is assumed small compared to that of ^{94}Zr, and we ignore it completely in the calculation. The σ and $\hbar\omega$ for ^{81}Br is obtained by a subbarrier-fusion fit for $^{81}Br+^{90}Zr$. Then we investigate the isotopic effects of Zr. As can be seen, the

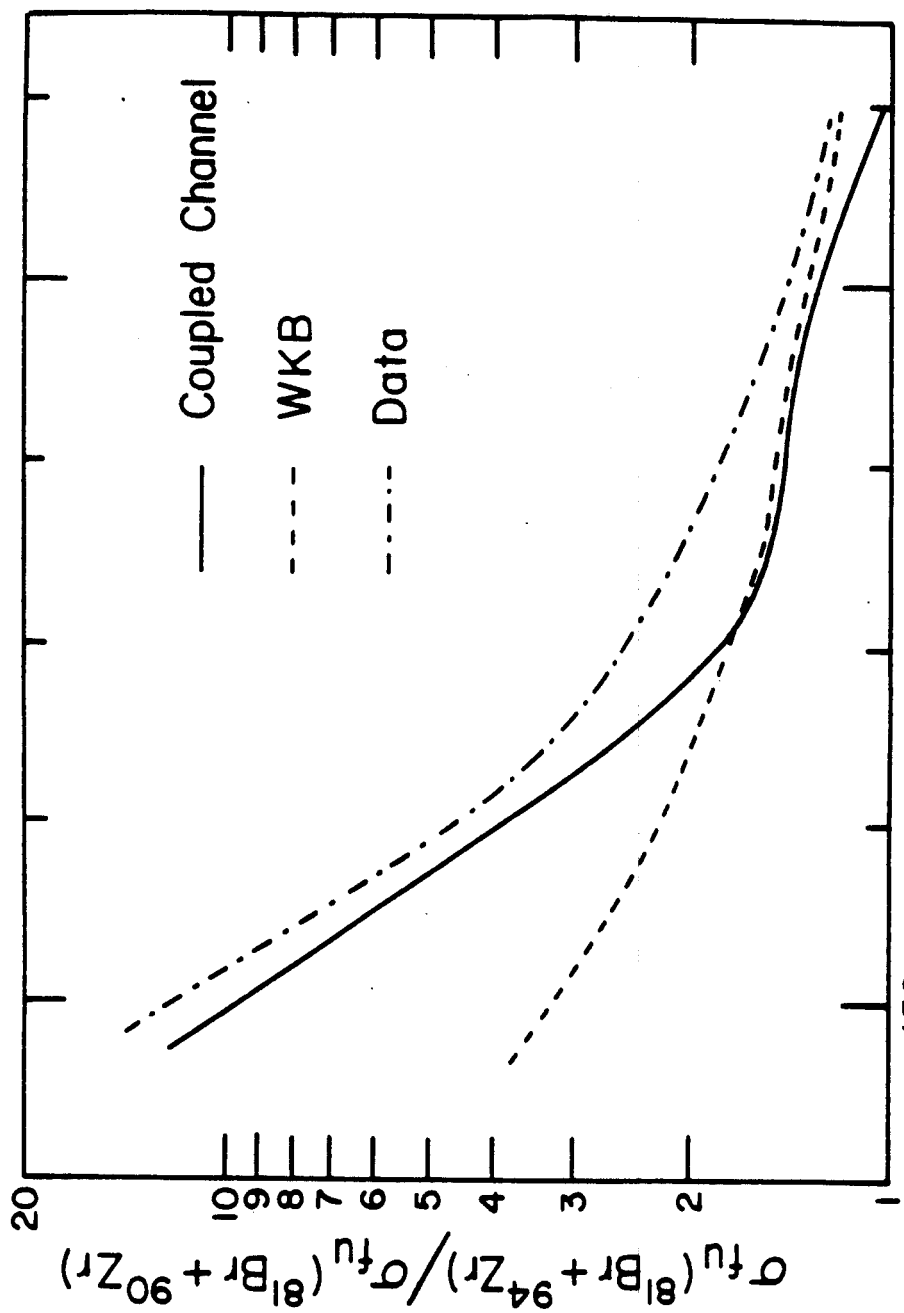

Fig.6.6. Plot of the ratio of the fusion cross sections for $^{81}Br+^{94}Zr$ to that for $^{81}Br+^{90}Zr$. The experimental data is the cross section of evaporation residue formation.

coupled-channel calculations which include the excitation in ^{94}Zr (solid line, reproduce the data reasonably well. While the results obtained by treating both ^{90}Zr, ^{94}Zr as point particles with the rescaled potential for the $^{81}Br+^{94}Zr$ system according to eq.(3.2) and eq.(3.3) are far away from being in agreement with the data in the subbarrier region. The above-barrier fusion is overpredicted by our coupled-channel calculation.

In these heavy systems the extra-push energies are zero for s-waves, but not for higher partial waves. The maximum ℓ-value with zero extra-push energy is about 26 (Bir.83), and one should take this into account in coupled-channel calculations. This was not done in our calculation, because only first few partial waves contribute for subbarrier fusion reactions.

Inside the Coulomb barrier, instead of fusing together, the system may transfer a few nucleons and then fall apart. In this case a so-called an "extra-extra-push" energy is needed for compound nucleus formation (Bir.83). In the systems $^{81}Br+^{90,94}Zr$, the extra-extra-push energies are not zero. This should affect the above-barrier fusion as well as subbarrier fusion. In the following, we explain why we believe that the relative subbarrier fusion can be investigated in our simple two-dimensional model, without treating these extra-push or extra-extra-push energies explicitly. In the calculation, we impose an incoming wave boundary condition at internuclear distance r_0 where the potential is the minimum in the entrance channel. For subbarrier fusion this is a reasonable approximation because as the system reaches r_0 it is unlikely to "bounce" back, and go through another penetration. The situation is quite different when the energy in the relative motion is greater than

the barrier height. The system energetically prefers to go to other channels rather than to complete fusion, if the energy is greater than the barrier height but not enough to overcome the extra-push (or extra-extra-push) barrier. However, the isotopic difference in extra-push energies in Zr should be small. When we fit subbarrier fusion for $^{81}Br+^{90}Zr$, the extra-push effects are accounted for by adjusting the σ and $\hbar\omega$ for ^{81}Br in subbarrier region. With such a σ and $\hbar\omega$ for ^{81}Br the subbarrier fusion difference between $^{81}Br+^{90}Zr$ and $^{81}Br+^{94}Zr$ should mainly be due to the isotopic difference in Zr. Because of the complexity, the extra-push effects explicitly show up in above-barrier energy region. These are qualitative arguments. In order to get a better agreement with the data, one has to perform much more complicated calculations in which many channels has to be included explicitly. This is beyond the scope of this thesis.

We also calculated the fusion cross sections for the systems $^{90}Zr+^{90}Zr$ and $^{94}Zr+^{90}Zr$. The parameters V_0, a, and ΔR are fixed by fitting the subbarrier fusion of $^{90}Zr+^{90}Zr$. With these potential parameters, however, the coupled channel calculations for $^{94}Zr+^{90}Zr$ underestimate the subbarrier fusion by about two orders of magnitude at the lowest energy measured. We believe that the particle transfers in $^{94}Zr+^{90}Zr$ reactions may contribute to the subbarrier fusion significantly, and account for the differences between the coupled channel calculations and the data (Bro.83).

We see that subbarrier fusion for systems below the extra-push threshold can be quantitatively understood by a two-dimensional model. For heavier systems that require an extra-push for fusion, the simple two-dimensional model can reproduce the relative fusion cross section

for different isotopes. The absolute fusion cross section, however, cannot be predicted by the model.

Chapter 7 Particle Transfers in Subbarrier Fusion

In this chapter, we study the effects of particle transfer on subbarrier fusion. The systems considered here are $^{58}Ni+^{58}Ni$ and $^{58}Ni+^{64}Ni$. In general, a complete calculation is numerically very difficult. But we make a simplified estimate, aiming to obtain results which give the right order of magnitude for subbarrier fusion.

7.1 Introduction

When two nuclei approach each other in a collision, a few nucleons may be transferred from one nucleus to another. This in general does not contribute very much to subbarrier fusion because of the small coupling amplitude. This is especially true for medium heavy or light systems where a small neck is enough to guarantee complete fusion. Particle transfers, however, may be important for systems which nave positive Q-values (Bro.83). Although the coupling strength for transfer is small, the subbarrier fusion cross section may be enhanced because the effective barrier in the transferred channel is lower than that in the entrance channel. For energies well below the Coulomb barrier, the small portion of the incoming flux in the transferred channel has a much larger penetration probability, leading to an enhancement in the fusion cross section. For some systems, there may be a large number of transfer channels coupled to the relative motion, and although the contribution due to each channel coupling is small, the enhancement due to all channel couplings may be significant (Rho.85).

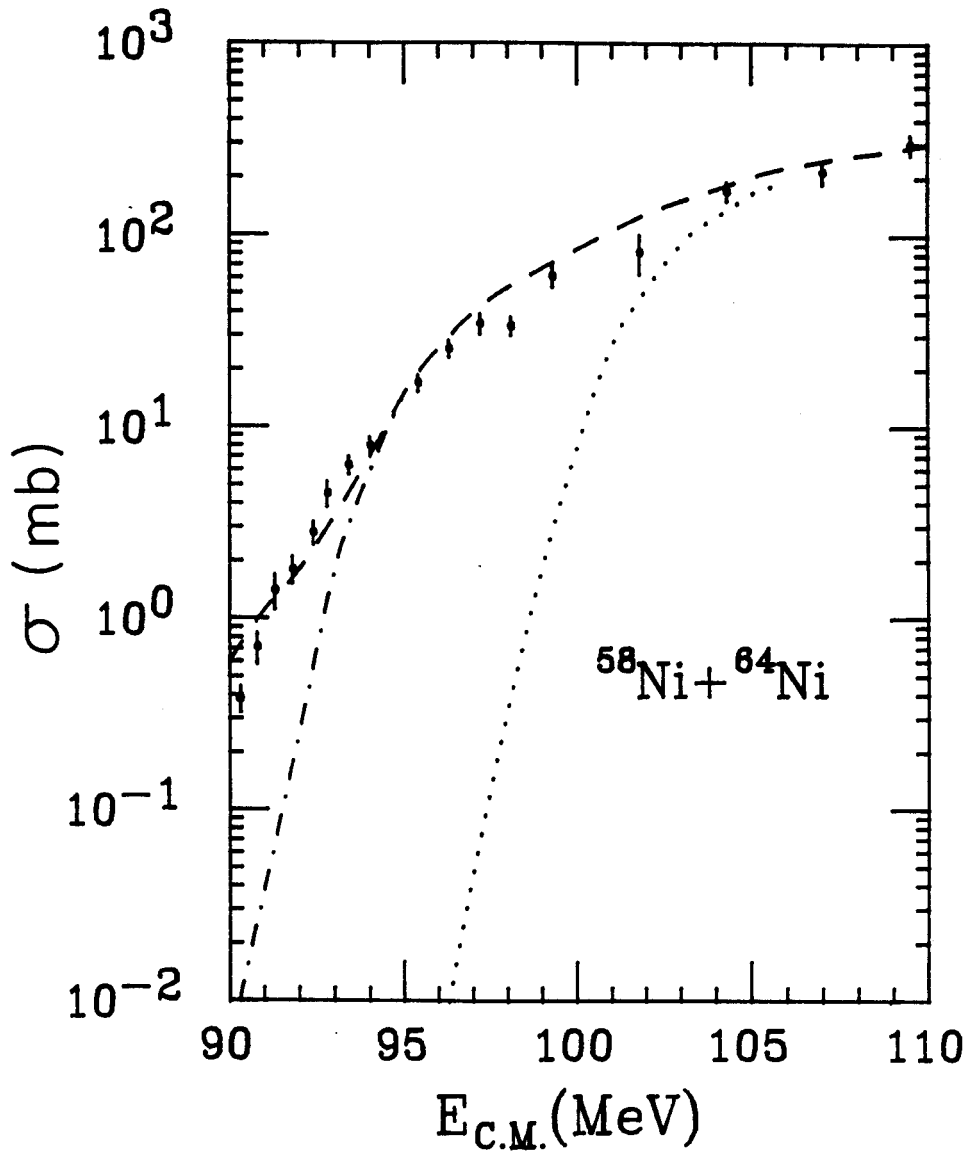

Fig.7.1. Calculated fusion cross sections for ^{58}Ni+^{64}Ni compared to the data of ref.(Bec.80). This plot is the copy of Fig.2(b) in ref.(Bro.83). The dotted curve shows the limit of no-coupling, i.e. one-dimensional barrier penetration. The dash-dotted curve is the result obtained by including intrinsic excitations. The dashed curve includes additional (1 MeV) strength at Q = +5 MeV, which was attributed to transfer reaction channels.

In comparing ^{58}Ni+^{58}Ni fusion data with that of ^{64}Ni+^{58}Ni, Broglia et al. (Bro.83) found that in addition to the known low-lying intrinsic excitations, an extra channel coupling with a positive Q-value was needed to reproduce the ^{64}Ni+^{58}Ni data. They found that a phenomenological constant coupling of 1 MeV strength and a Q-value of 5 MeV was required. With this additional channel coupling, the relative enhancement in the ^{64}Ni+^{58}Ni fusion cross section was explained, and is shown in Fig.7.1.

From Fig.7.1, one see that with all known low-lying excitations coupled (dashed curve), the fusion is still underestimated at energies far below the Coulomb barrier. But good agreement is obtained with the additional coupling (continuous curve). This additional channel coupling was interpreted as being due to two-neutron transfer (from ^{64}Ni to ^{58}Ni) for which the Q-value is positive.

It would be nice if the additional channel coupling can be understood microscopically. In the following sections, we will study a microscopic model for the two-neutron transfer form factor in the ^{58}Ni+^{64}Ni system and its effects on subbarrier fusion.

7.2 Form Factors for Neutron Transfer

In our microscopic treatment, the neutron-transfer form factor is calculated as

$$f_i(j_1,j_2;j_1',j_2';r)=\langle {}^{A-i}\psi_{j_1}\ {}^{A'+i}\psi_{j_2}|V|{}^{A-i+1}\psi_{j_1'}\ {}^{A'+i-1}\psi_{j_2'}\rangle, \qquad (7.1)$$

where $|^{A}\psi_{j}>$ is the many-particle wave function for a Ni-isotope with a spin j, and V is the single-particle potential field in the nucleus to which the neutron is transferred. Also, i=1 and i=2 label first- and second-neutron transfer, respectively. The ground states of ^{58}Ni, ^{60}Ni, ^{64}Ni and ^{62} Ni have $J^{\pi}=0^{+}$ and the trivial indices indicating these nuclei will be suppressed. Since V is a one-body operator, the form factor can be written in second quantization form as

$$f_1(j_1,j_2;r) = \sum_{\ell;k} \langle k|V|\ell\rangle \langle {}^{63}\psi_{j_1}|a_\ell|{}^{64}\psi\rangle \langle {}^{59}\psi_{j_2}|a_k^\dagger|{}^{58}\psi\rangle$$

$$f_2(j_1,j_2;r) = \sum_{p;q} \langle q|V|p\rangle \langle {}^{62}\psi|a_p|{}^{63}\psi_{j_1}\rangle \langle {}^{60}\psi|a_q^\dagger|{}^{59}\psi_{j_2}\rangle \quad , \qquad (7.2)$$

where $|k>$, $|\ell>$, $|q>$ and $|p>$ represent single-particle states in ^{58}Ni, ^{64}Ni, ^{59}Ni and ^{63}Ni, respectively.

For ^{59}Ni+^{63}Ni, there are 3 low-lying levels in each nucleus, $j=(\frac{1}{2}^-, \frac{3}{2}^-, \frac{5}{2}^-)$ for a total of 12 states (including m-degeneracy), and, therefore, there are 144 different internal states for the ^{59}Ni+^{63}Ni system. Conservation of the angular momentum along the axis connecting the two nuclei reduces this quantity to 28. However, this is still too large because of the numerical difficulties in carrying out the calculation. We shall make the approximation that these internal states are degenerate, and can be treated as one state. From second-order perturbation theory, the form-factor for one-neutron transfer is given by

$$F(r)=\sqrt{\sum_I \langle f|V|I\rangle\langle I|V|i\rangle} = \sqrt{\sum_{j_1,j_2} f_1(j_1,j_2;r) f_2(j_1,j_2;r)} \qquad (7.3)$$

for both first- and second-neutron transfer. This is a good approximation only when the Q-value for the first-neutron transfer is large and negative (that is, first-order perturbation gives little contribution). This, however, is not the case. Therefore, the form factor $F_1(r)$ for first-neutron transfer is the square root of the sum of the squares of each individual form factors, that is,

$$F_1(r)=\sqrt{\sum_I \langle I|V|i\rangle^2} = \sqrt{\sum_{j_1,j_2} f_1(j_1,j_2;r)^2} \tag{7.4}$$

as one would expect from the first-order perturbation theory. While the form factor for second-neutron transfer is

$$F_2(r)=F^2(r)/F_1(r). \tag{7.5}$$

The Q-values for one- and two-neutron transfer are taken from binding energy data (Bro.83) and are -0.6 MeV and 3.9 MeV, respectively. We assume that the neutrons are transferred one by one, i.e., no simultaneous two neutron transfer. We will see later that this is indeed a reasonable approximation.

7.3 Details of the Calculation

Both ^{58}Ni and ^{64}Ni are open-shell nuclei, and intrinsic collective motions are important in subbarrier fusion. In order to reproduce the fusion data, these couplings are needed along with the neutron transfer coupling. However, since we are primarily interested in the effects due

to neutron transfer, we parameterize the intrinsic collective excitations by fitting the fusion excitation function data in $^{58}Ni+^{58}Ni$. The potential is again that of eq.(3.2). The strength V_0, the barrier shift ΔR, and the diffuseness a are parameters to be determined.

The intrinsic excitations are characterized by a harmonic-oscillator spectrum in the variable s, with a r. m. s. amplitude σ and excitation energy $\hbar\omega$. We first fit the $^{58}Ni+^{58}Ni$ fusion data by adjusting these parameters. This is done using the coupled-channel technique, where the number of channels is also a parameter in the fit. The resulting parameters are shown in Table 7.1. This two-dimensional

Table 7.1 Parameters of the two-dimensional potential (eq.(3.2)) and the surface harmonic-vibrational mode obtained by fitting the $^{58}Ni+^{58}Ni$ fusion data.

V_0	a	No. of surface vibrational states	σ (The r. m. s. amplitude of s in the ground state)	$\hbar\omega$
-36 Mev	0.7 fm	3	0.4 fm	3 MeV

potential is then used for the $^{58}Ni+^{64}Ni$ system, where corrections due to the larger size of ^{64}Ni are applied. In doing this, we actually assume that the intrinsic couplings are the same for both the $^{58}Ni+^{58}Ni$

and $^{58}Ni+^{64}Ni$ systems. We justify this assumption by comparing our results with those obtained with the more detailed treatment of Broglia et al. (Bro.83) (without neutron transfer). We find generally good agreement between the two procedures for energies far below the Coulomb barrier.

In our calculation, the potential fields which generate the single particle orbits and cause the neutron transfers are assumed to have a Woods-Saxon form. The parameters used are those given by Bohr and Mottelson (Boh.69). The spectroscopic factors, used in eq.(7.2), were calculated with the Oxford-Buenos Aires-MSU Shell-Model Code (Rae.85) using the fp-shell interaction of van Hees (Van.81) and Koops (Koo.77). The shell-model configuration space consisted of the $0f_{7/2}$, $1p_{3/2}$, $0f_{5/2}$ and the $1p_{1/2}$ orbits. Due to computational restrictions, no particle-hole excitations of the closed $0f_{7/2}$ orbit were allowed. In addition, corrections to eq.(7.2) due to the non-orthogonality of single particle states in different nuclei have been neglected since the overlaps are small. The form factors are shown in Fig.7.2.

When particle transfer and internal excitation are coupled with the relative motion, the subbarrier fusion cross-section is greatly enhanced. This can be seen in Fig.7.3. The dot-dashed curve is the result obtained by including both intrinsic excitation and the neutron-transfer couplings (three-dimensional calculations), and is greater than the result obtained with only the intrinsic-excitation couplings (dashed line), which is, in turn, much greater than the result given by the one-dimensional barrier penetration model (dotted line). There is, however, still a gap between this calculation and the experimental data for energies far below the Coulomb barrier.

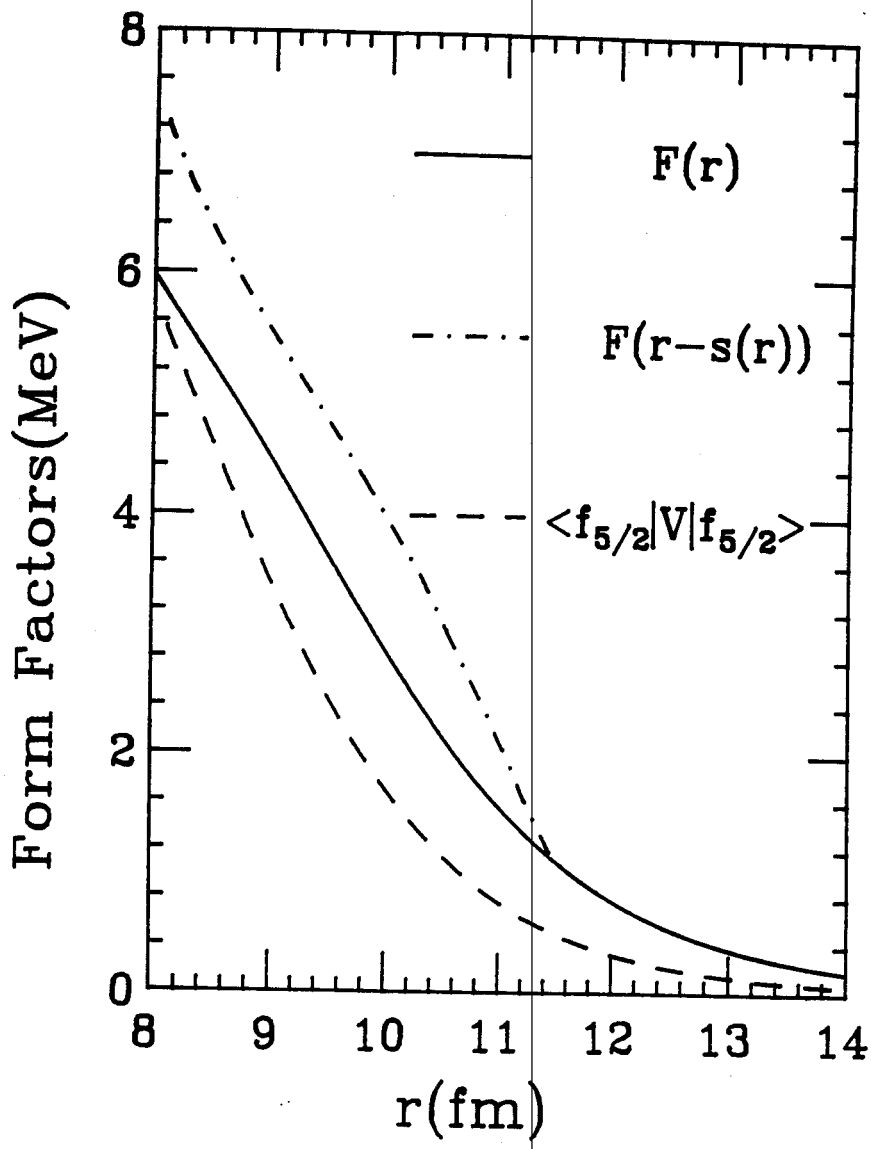

Fig.7.2. Form factor F(r)(solid line) is shown as function of the separation r. F(r-s(r))(dot-dashed curve) is the form factor in the semiclassical model. Also shown (dashed curve) is the largest single-particle transfer amplitude between two $f_{5/2}$ orbits in ^{64}Ni and ^{58}Ni, respectively.

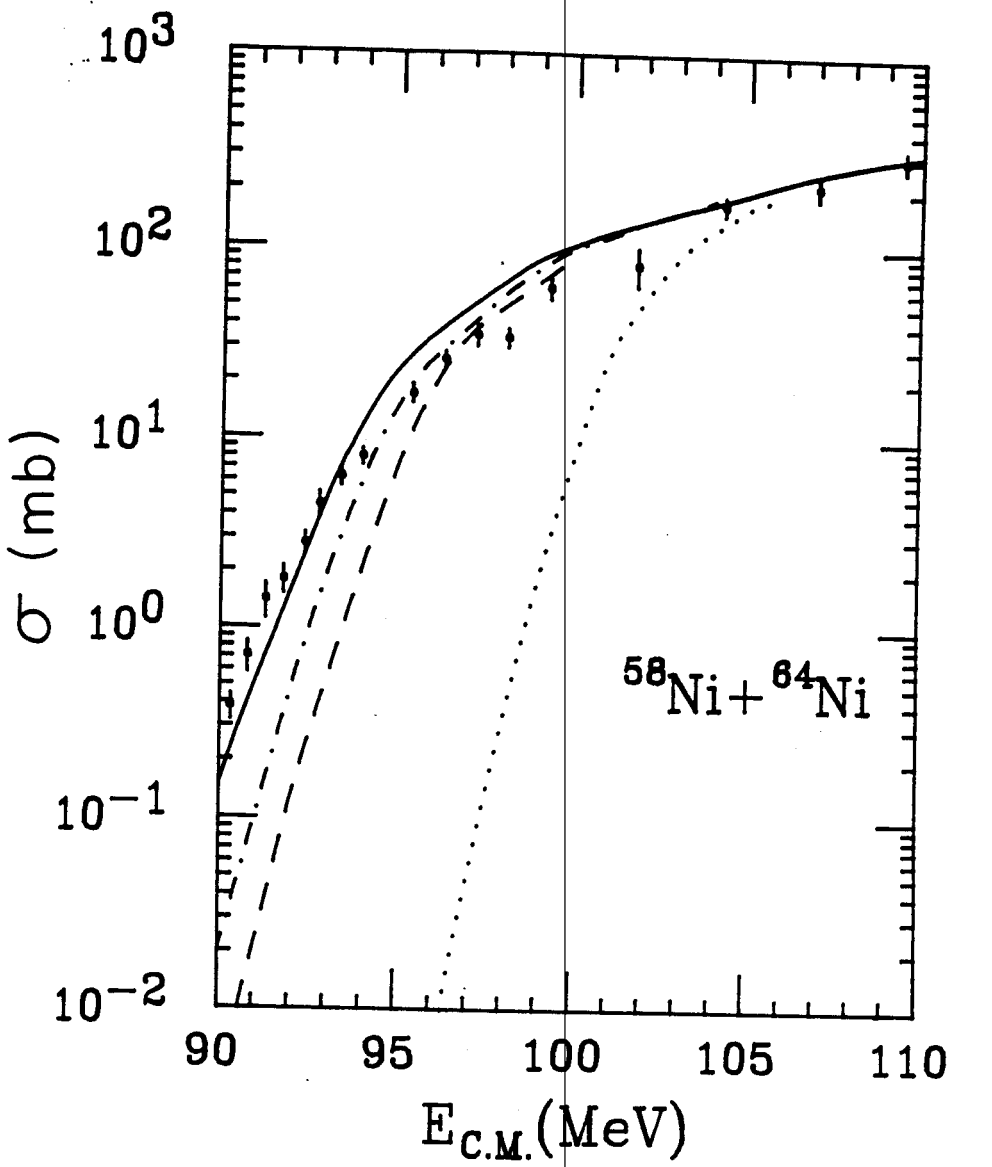

Fig.7.3 Fusion excitation functions of the ^{64}Ni+^{58}Ni system. Dotted curve is the result of the one-dimensional barrier penetration model. The dashed curve is the result obtained by including only intrinsic excitations with parameters given in Table 7.1. The dot-dashed curve is the result with both transfer and intrinsic excitation included. The $F_i(r-s(r))$'s are the form factors used in obtaining the result that reproduces data (solid line).

7.4 The Interplay of Intrinsic Excitations and the Particle Transfers on Subbarrier Fusion

The particle-transfer form factor was evaluated using eq.(7.2) for nuclei in their ground states. However, the nuclei may be deformed during the collision, with a preferred deformation such that the long axis coincides with the axis connecting the two nuclei. This effect enhances the neutron-transfer form factor because the nuclei are effectively closer than they are in their ground state. We take this into account by evaluating eq.(7.2) along a semiclassical trajectory. First, turning off the neutron transfer, we perform a two-dimensional penetration calculation using the potential defined in eq.(3.2) and the parameters in Table 7.1. The semiclassical trajectory is defined as that in which the incoming flux is maximized in the direction of the surface-vibrational degree of freedom, parameterized by s, and is shown in Fig.7.4. In a semiclassical approximation, we assume that the system only goes through this trajectory, and therefore, the form factor $F_i(r)$ is replaced by $F_i(r-s(r))$, $s(r)$ being evaluated on the trajectory. With this enhanced form factor, we find general good agreement between theory (solid curve in Fig.7.3) and experiment. We note, however, that the experimental data are underestimated somewhat for low energies.

7.5 Simultaneous Two Neutron Transfer

So far, we have neglected the simultaneous two-neutron transfer mediated by the residual interaction. We estimate this contribution by

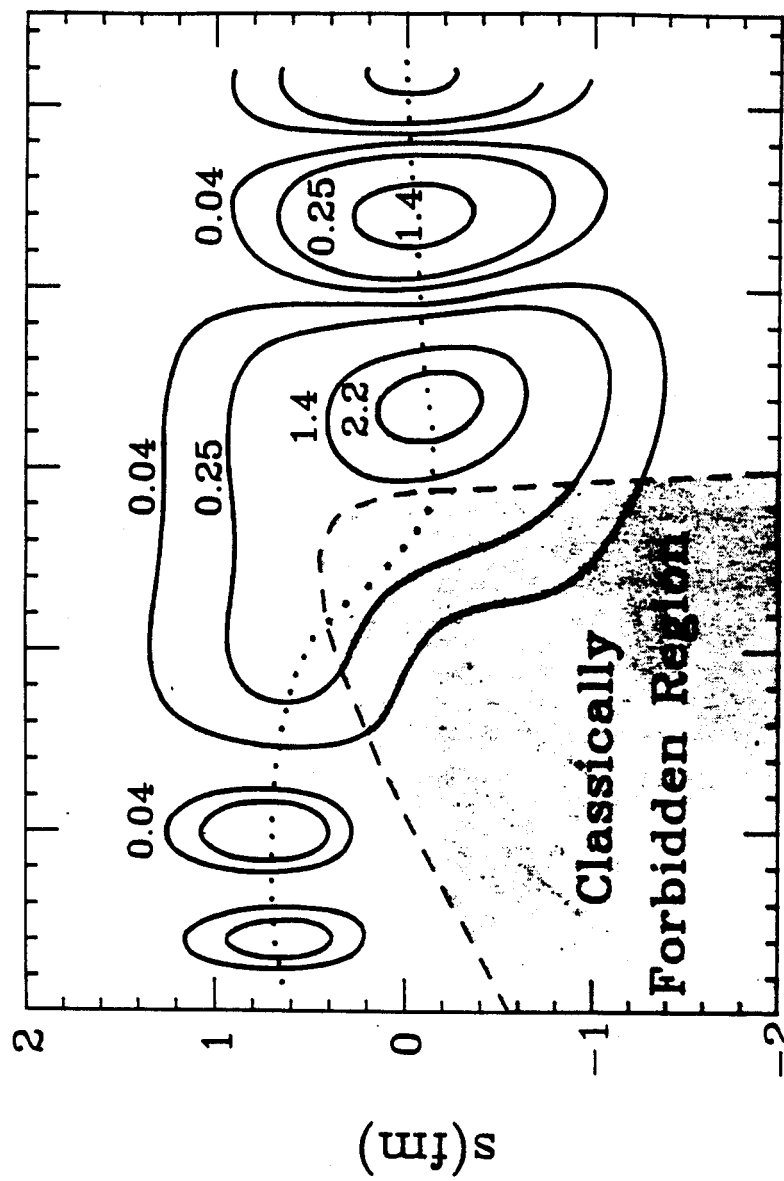

Fig.7.4. Contours of equal density $|\psi(r,s)|^2$ are shown in the (r,s) plan. The wave function is the coupled-channel result without transfer coupling for the reaction $^{58}Ni+^{64}Ni$ at a c.m. energy of 90 MeV with parameters given in Table 7.1. The dotted curve is the semiclassical trajectory in which the incoming flux is maximized in the s-direction.

assuming the residual interaction to have a δ-function dependence, whose strength is determined from the pairing energy in ^{58}Ni. This residual interaction coupled with shell-model two-particle parentage coefficients yields two-neutron transfer form factors which change the fusion cross section by only a few percent.

The residual interaction in ^{58}Ni may be much more complicated in form than the δ-function pairing described above. However, we believe that the above pairing is the leading part of the residual interaction. The above procedure should, at least, give the correct order of magnitude of the effects due to simultaneous two-neutron transfer.

7.6 Discussions

We find that the relative enhancement of the ^{58}Ni+^{64}Ni fusion cross section over that of ^{58}Ni+^{58}Ni is explained in our simple model (see Fig.7.3). However, the calculation should only be taken seriously to within a factor of two or so, as there are a few uncertainties in the model. First, the intrinsic excitations in ^{64}Ni are not identical to those of ^{58}Ni, although at energies far below the Coulomb barrier, our results (with intrinsic coupling only) agree with those obtained with the more detailed analysis of Broglia et al. Second, the 28 one-neutron transferred states were treated as one intermediate state. Third, the replacement F(r) with F(r-s(r)) is a semiclassical approximation. Finally, the neutron-transfer form factors were evaluated using eg.(7.2) with shell-model spetroscopic factors. There is evidence (Bay.82), however, that this procedure may in fact underestimate contributions due to step-by-step two-neutron transfer. Since two-neutron transfer is

very important at low energy, this may explain the discrepancy between theory and experiment at low energy (see Fig.7.3).

It should be remarked that the system $^{58}Ni+^{64}Ni$ is nearly symmetric, with only a few transfer channels contributing towards fusion. However, in order to get more comprehensive appreciation of the effects due to particle transfer on subbarrier fusion, a systematic study of asymmetric systems where many particle-transfer channels are open is necessary.

After extensive experimental and theoretical studies over past a few years, the effects due to intrinsic excitations on heavy-ion subbarrier fusion are well understood qualitatively. Quantitative agreements can now be achieved in many cases. For light and medium systems, coupled channel methods give a satisfactory description of subbarrier fusion. However, there are some ambiguities associated with choice of the parameters. As is discussed by Rhoades-Brown et al. (Rho.84), these uncertainties maybe reduced by constraining the parameters to reproduce other data, such as inelastic and elastic scattering, etc. There are no free parameters for neutron-transfer form factor in our calculation. The parameters that come from a shell model give the neutron-transfer form factors which describe subbarrier fusion. It is also important to verify that the transfer form factors in this work are consistent with data on the particle transfer reactions. This has been measured in the Ni+Ni system (Van.86) and the analysis is under way (Lan.86).

Chapter 8 Conclusions

The structure effect on subbarrier fusion was first described by ZPM. ZPM provides a simple picture of the interplay between intrinsic degree of freedom and internuclear motion. Also, calculations in ZPM are easy. We found that ZPM is a good approximation for describing low-lying intrinsic excitation effects on subbarrier fusion in medium heavy systems (Fig.4.1). In general, ZPM gives the right order of magnitude of the effects due to low-lying collective excitations. To describe subbarrier fusion more accurately, however, finite energy excitation formulation (coupled channel method) is needed in some systems (Fig.6.2).

In light systems, only the first few intrinsic excitations need to be included in the two-dimensional model to describe subbarrier fusion because of the relatively large excitation energies. Structure effects on subbarrier fusion in light systems can therefore be described well without ambiguities in the theory (Fig.5.1,2). In the case of $^{18}O+^{16}O$, only the transition from the ground state to the first excited state in the ^{18}O is treated in the theory. In medium heavy systems, more intrinsic excitations are needed in the model space in order to describe subbarrier fusion (Fig.6.2). Subbarrier fusion in medium systems can also be well understood in the two-dimensional model with vibrational parameters close to those that describe low-lying collective excitations.

Particle transfers were found to be important in the subbarrier fusion of $^{64}Ni+^{58}Ni$ in a macroscopic model (Bro.83), and is also well explained using the microscopic model of this work.

References

Bal.83 A. B. Balantekin, S. E. Koonin, J. W. Negele, Phys. Rev. **C28** (1983) 1565

Bay.82 B. F. Bayman and Jongsheng Chen, Phys. Rev. **C26** (1982) 1509

Bec.81 M. Beckerman, M. Salomaa, A. Sperduto, H. Enge, J. Ball, A. DiRienzo, S. Gazes, Yan Chen, J. D. Molitoris and Mao Nai-feng, Phys. Rev. Lett. **45** (1980) 1472

Bec.84 M. Beckerman, J. Wiggins, H. Aljuwair, and M. K. Salomaa, Phys. Rev. **C29** (1984) 1938

Bir.83 J. R. Birkelund and J. R. Huizenga, Ann. Rev. Nucl. Part. Sci. **33** (1983) 265

Blo.71 R. Blocki, Randrup, W. H. Swiatecki and C. F. Tsang, Ann. of Phys. **105** (1977) 427

Boh.69 A. Bohr and B. Mottelson, Nuclear Structure Vol. I, W. A. Benjamin, Inc. 1969

Bro.75 R. Broda, M. Ishihara, B. Herskind, H. Oeschler, S. Ogaza and H. Ryde, Nucl. Phys. **A248** (1975) 356

Bro.83 R. A. Broglia, C. H. Dasso, S. Landowne, G. Pollarolo, Phys. Lett. **133B** (1983) 34

Chr.76 P. R. Christensen and A. Winther, Phys. Lett. **61B** (1976) 113

Esb.81 H. Esbensen, Nucl. Phys. **A352** (1981) 147

Esb.83 H. Esbensen, J. Q. Wu and G. F. Bertsch, Nucl. Phys. **A411** (1983) 275

Gut.73 H. H. Gutbrod, W. G. Winn, and M. Blann, Nucl. Phys. **A213** (1973) 267

Hil.53 D. L. Hill and J. A. Wheeler, Phys. Rev. **89**(1953)1102

Koo.77 J. E. Koops and P. W. M. Glaudemans, Zeits. f. Physik **A280** (1977) 181

Lan.81 S. Landowne and H. H. Wolter, Nucl. Phys. **A351** (1981) 171

Lec.84 Lecture Notes in Physics **219** (1984)

Lan.86 S. Landowne, private communication.

Nat.70 J. B. Natowitz, Phys. Rev. **C** 1 (1970) 623

Nix.77 J. R. Nix and A. J. Sierk, Phys. Rev. **C15** (1977) 2072

Püh.75 F. Pühlhofer, W. Pfeffer, B. Kohlmeyer and W. F. W. Schneider, Nucl. Phys. **A244** (1975) 329

Rae.85 W. D. M. Rae, A. Etchegoyen, N. S. Godwin, and B. A. Brown, OXBASH, The Oxford-Buenos Aires MSU Shell-Model Code, Michigan State University Cyclotron Laboratory report #524

Rho.80 M. Rhoades-Brown, M. H. Macfarlane and Steven C. Pieper, Phys. Rev. **C21** (1980) 2417.

Rho.84 M. J. Rhoades-Brown, P. Braun-Munzinger, M. Prakash and S. Sen in Lecture notes in physics, vol. **219** (1984) p. 162

Rho.85 M. A. Rhoades-Brown, private communication

Rin.78 P. Ring, H. Massmann and J. Q. Rasmussen, Nucl. Phys. **A296** (1978) 50

Sch.68 Leonard I. Schiff, Quantum Mechanics, p278, 1968, MacGraw-Hill, Inc.

Ste.85 P. Stelson, private communication

Sto.78 R. G. Stokstad et al., Phys. Rev. Lett. **41** (1978) 465

Swi.81 W. J. Swiatecki, Physica Scripta **24** (1981) 113, and Nucl. Phys. **A376** (1981) 275

Tak.85 N. Takigawa and K. Ikeda, Tohoku Univ., preprint, 1985

Tan.85 O. Tanimura, J. Makowka and U. Mosel, Phys. Lett. **163B** (1985) 317

Tho.85 J. Thomas et al., Phys. Rev. **C31** (1985) 1980

Van.81 A. G. M. Van hees and P. W. M. Glaudemans, Zeits. f. Physk **A303** (1981) 267

Van.86 A. M. van den Berg, et al., Phys. Rev. Lett. **56** (1986)572

Won.73 C. Y. Wong Phys. Rev. Lett., **31** (1973) 766

Wu.86 J. Q. Wu and G. F. Bertsch, Michigan State Univ., preprint 1986